Journal of *Marine Science and Engineering*

MDPI

Article

Factors Controlling the Pore Development of Low-Mature Marine–Continental Transitional Shale: A Case Study of the Upper Permian Longtan Shale, Western Guizhou, South China

Manting Zhang [1], Mingyi Hu [1,*], Sile Wei [1], Quansheng Cai [1], Wei Fu [1], Fang Shi [2], Lei Zhang [3] and Haiyan Ding [2]

[1] School of Geosciences, Yangtze University, Wuhan 430100, China; 2021730041@yangtzeu.edu.cn (M.Z.)
[2] Research Institute of Exploration and Development of Tarim Oilfield Company, PetroChina, Korla 841000, China
[3] Lunnan Oil and Gas Production Management Zone of Tarim Oilfield Company, PetroChina, Korla 841000, China
* Correspondence: hmy_1965@163.com

Abstract: The Upper Permian Longtan Shale is a significant reservoir in western Guizhou. To clarify the main factors controlling the low-mature marine–continental transitional shale pore development in western Guizhou, pore types were classified with scanning electron microscopy (SEM), and the pore developmental stages and morphological structures were quantitatively characterized by nitrogen adsorption isotherm analyses. Additionally, the qualitative or semi-quantitative relationships between the pore developmental stages and the main controlling factors were established via geochemical analysis. The results showed that the Longtan Shale pores include intergranular pores, intragranular pores, organic pores, and microfractures. The intergranular pore structures were categorized into ink-bottle, slit, layered, and irregular types. The intragranular pores were found to be of the elliptical, nearly circular, ink-bottle, and irregular varieties. The organic pores were categorized into elliptical, bubble-like, and irregular polygonal variants. The microfractures were only of the elongated type. The clay-mineral-related intergranular pores were the predominant pore type. The organic pores were found to be poorly developed. The mesopores were predominant, followed by macropores. The shale pore diameters ranged between 1 nm and 100 nm, and they are characterized by multiple peaks. The specific surface area (SSA) was primarily provided by nanopores in the range of 5 nm to 10 nm, such that the smaller pores provided a greater contribution to the SSA, and they are more conducive to shale gas adsorption and accumulation. Clay mineral content was the dominant internal factor controlling pore development and the SSA, with the illite–smectite mixed layer being the most obvious controlling factor. While too low or too high clay mineral content is adverse to macropore development, brittle mineral content, carbonate mineral content, and total organic carbon (TOC) content are adverse to pore development and the SSA. Thermal maturity has no remarkable control effect on pore volume and the SSA of non-organic pores.

Keywords: western Guizhou; the Longtan Shale; shale pore; low mature; development characteristics; controlling factors

check for updates

Citation: Zhang, M.; Hu, M.; Wei, S.; Cai, Q.; Fu, W.; Shi, F.; Zhang, L.; Ding, H. Factors Controlling the Pore Development of Low-Mature Marine–Continental Transitional Shale: A Case Study of the Upper Permian Longtan Shale, Western Guizhou, South China. *J. Mar. Sci. Eng.* **2023**, *11*, 1862. https://doi.org/10.3390/jmse11101862

Academic Editor: Michael Lazar

Received: 1 September 2023
Revised: 21 September 2023
Accepted: 24 September 2023
Published: 26 September 2023

Copyright: © 2023 by the authors. Licensee MDPI, Basel, Switzerland. This article is an open access article distributed under the terms and conditions of the Creative Commons Attribution (CC BY) license (https://creativecommons.org/licenses/by/4.0/).

1. Introduction

Shale gas is a clean and efficient energy source; thus, it is highly valued by countries around the world. China has taken a quantum leap in marine-shale commercial exploration, mainly with respect to the marine shale found in the Wufeng–Longmaxi Formation in the Sichuan Basin and its periphery, which has formed the Weiyuan, Changning, Fuling, and other shale gas fields [1–3]. There are multiple types of shale developed in southern China, such as marine shale, marine–continental transitional shale, and continental shale. Unlike marine shale, the cumulative thickness of marine–continental transitional shale in western

Guizhou is large, but the single layer is thin. The single layer is usually between 5 m and 15 m. In the longitudinal direction, the lithology changes rapidly. The shale interval is often associated with tight sandstone or coal seams, with the longitudinal distribution characteristics of gas-bearing coal rock, shale, and gas-bearing tight sandstone interbeds, which have rich shale gas resource potential [4]. However, most of the shale pore research focuses on the marine shale of the Wufeng–Longmaxi Formation, and less attention is paid to the marine–continental transitional shale of the Longtan Formation. The marine-shale exploration practice of the Wufeng–Longmaxi Formation reveals that shale pores play a significant role in controlling shale gas enrichment [5]; thus, it has momentous significance in terms of characterizing pore structure [6–9]. As such, in this study, the main controlling factors of pore development are explored.

Many scholars have proposed various classification schemes for shale pores. The International Union of Pure and Applied Chemistry (IUPAC) classified shale pores, based on pore diameter, into micropores, mesopores, and macropores. This classification scheme is extensively used in the quantitative description and rating of reservoir pores. When studying the siliceous Barnett shale in Fort Worth Basin, North America, Loucks et al. (2012) proposed that matrix pores can be classified into organic pores, intragranular pores, and intergranular pores according to their location relationship between pores and particles [10], but this classification scheme did not include microfractures. Yu Bingsong conducted a comprehensive classification based on two parameters: pore diameter and pore occurrence. In accordance with the relationship between mineral particles and pores, shale pores can be classified into matrix pores and microfractures [11]. The matrix pores can be classified into organic pores, intragranular pores, and intergranular pores. A proposal for the classification of the pore types according to pore morphology, including cylindrical pores, ink-bottle pores, funnel-shaped pores, and slit pores, was put forward by Rouquerol et al. (1994) [12]. The main pore types that develop in different shale types are also different. Marine-shale organic matter is mainly composed of sapropelinite in a large number of organic pores, while the marine–continental transitional shale and continental shale consist chiefly of vitrinite with poor organic pores. The main factors controlling pore development comprise TOC content, thermal evolution degree, kerogen type, mineral composition, etc. It is generally believed that shale porosity increases along with increases in the organic carbon content and maturity, but certain scholars have proposed a different view: When the maturity is low, the liquid hydrocarbons generated from organic matter can block some pores, thus causing a decrease in the effectively connected pores. It has been found that not all organic matter types can form nanoscale organic pores [13–15]. Different from type III kerogen, type I and type II kerogen are more likely to develop organic pores under the same thermal-evolution degrees. This shows that sapropelinite is a favorable factor for organic pore development. In summary, there are various shale pore types and numerous controlling factors, and there are certain differences in the major controlling factors for shale pore structures under different geological backgrounds. Therefore, it is essential to study the shale pore structure and controlling factors under different geological backgrounds.

The Upper Permian Longtan Formation in Guizhou is a potential reservoir for shale gas exploration and development in South China, and it has received widespread attention in recent years. Influenced by multi-stage geological tectonics, the reservoir lithological assemblages and pore structure are complex, and they are characterized by multiple layers, thin layers, large cumulative thicknesses, frequent interbedding, abundant organic matter, low maturity, and high clay mineral content. Though the existing literature has covered the shale pore structure characteristics [6,8,9,16–18], studies exploring areas such as low-mature marine–continental transitional shale pore structure characteristics and the dominant factors controlling shale pore development are lacking. In this research, the Longtan Shale core samples from the HP3 and YL4 wells in western Guizhou were selected. SEM was used to classify the pore types, and nitrogen adsorption isotherms quantified the pore developmental stages and morphological structures. Based on the geochemical test data of the kerogen types, TOC content, maturity, and mineral compositions of the shale

samples, the dominant factors controlling shale pore development of the Longtan Formation were defined. These research findings can provide valuable information and references for low-mature marine–continental transitional shale studies on pore characteristics, fine reservoir characterization, and shale gas potential.

2. Geological Setting

Western Guizhou is located in the southwest Guizhou Depression, which belongs to the southwest section of the Upper Yangtze Platform (Figure 1). It has undergone multiple stages and high-intensity tectonic evolution, mainly including the Himalayan Movement, Yanshan Movement, Indosinian Movement, Hercynian Movement, and the Caledonian Movement. Under the influence of these orogenic transformations, folds and faults are developed in western Guizhou, mainly in the form of barrier folds. Anticlines are generally cut by accompanying faults, and the open synclines enable most of the Longtan Formation strata to be preserved.

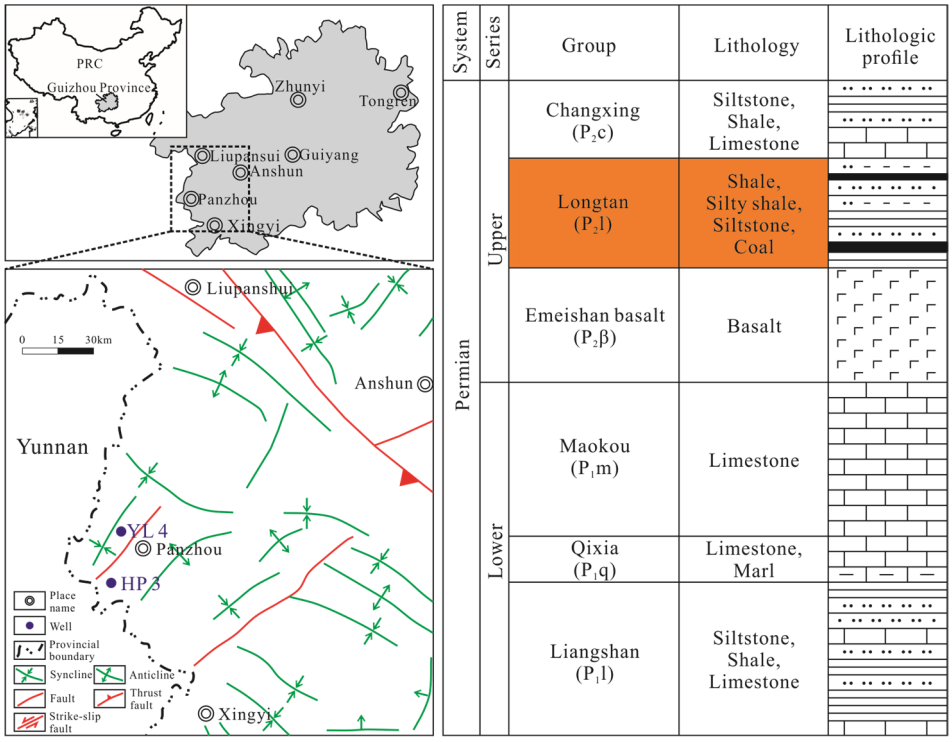

Figure 1. Structure outline map and the stratigraphic system in western Guizhou [19].

The Yangtze Platform experienced several transgression events on a large scale in the Paleozoic. Four shale sets were formed, represented by the Upper Permian, Lower Permian, Upper Ordovician–Lower Silurian, and Lower Cambrian sequences. During the Late Permian, the Longtan Shale was formed when the volcanic activity of the ancient Kangdian land weakened, and when periodical transgression occurred from eastern Guizhou to western Guizhou. A wide range of marine–continental transitional shale in the Longtan Formation was deposited, and the sedimentary environment mainly consisted of delta facies, tidal flat facies, and lagoon facies [19]. The stratum thickness was, generally, relatively large (150 m–300 m), with diverse lithology, which mainly included coal seams, siltstone, argillaceous siltstone, silty mudstone, and shale (Figure 1). Fine sandstone was seen occasionally with pyrite and thin layers of siderite. The Longtan Shale accumulated thickness varies from 30 m to 50 m, and it is characterized by multiple thin single layers and large accumulation thicknesses. It can be seen that the shale frequently alternates with sand and coal, which is the preferred layer series for shale gas exploration. The Longtan Shale is

at stage A of the mid-diagenetic stage, and the main types of diagenesis are compaction, cementation, recrystallization, dissolution, and alteration [20].

3. Samples and Methods

Due to the strong weathering of outcrop samples, it is difficult to truly reflect shale reservoir characteristics. The test and analysis samples in this study were collected from drilling cores, which were mainly dark gray silty mudstone, dark gray shale, and gray-black carbonaceous shale. Nineteen Longtan Shale samples were collected from the HP 3 and YL 4 wells in western Guizhou. The samples were studied via the TOC determination test, vitrinite reflectance analysis, kerogen maceral identification and type classification, X-ray diffraction and clay mineral analysis, argon ion polishing SEM, and a low-temperature nitrogen adsorption experiment.

This study used a CS-230 sulfur carbon analyzer for the TOC determination. The experiment was carried out at 25 °C and 60% RH. Vitrinite reflectance analysis, kerogen macerals identification, and type classification were carried out using a Scope.A1 microphotometer. The X-ray diffraction method was used to study the shale mineralogy. The experiment was carried out with an Ultima IV X-ray diffractometer. All the samples were ground into fine powder (i.e., less than 40 μm). Diffraction patterns can help with determining and semi-quantitatively analyzing the relative abundance of minerals. The shale samples were prepared using a Gatan 697 Ilion Type II wide-beam argon ion polishing instrument, observed with ZEISS SIGMA field emission SEM. The low-temperature nitrogen adsorption experiment was conducted with a Quadrascorb SI-specific surface analyzer at 20 °C and a 30% RH. The samples were heated at 90 °C for 1 h and at 350 °C for 5 h.

4. Results

4.1. Organic Geochemical Characteristics

4.1.1. Kerogen Type

There are differences in the hydrocarbon potential among different kerogen types. The maceral identification of the Longtan Shale organic matter shows that sapropelinite ranges between 2.00% and 25.00%, with an average of 8.89%. Exinite ranges from 5.00% to 46.00%, with an average of 20.11%. Vitrinite ranges from 27.00% to 89.00%, with a mean of 61.00%. Inertinite varies between 3.00% and 27.00%, with a mean of 10.00% (Table 1). Overall, vitrinite has the highest values, followed by exinite. The predominant type of kerogen is type III, followed by type II_2 (which has a tendency to generate gas).

4.1.2. TOC Content

Previous exploration practices show that shale with a high TOC content has good hydrocarbon potential. The industrial accumulation of shale gas requires a base of rich gas source material and a certain standard of hydrocarbon-generating organic matter content. Boyer (2006) believed that the shale TOC content should be at least 2% [21]. According to sample tests, the Longtan Shale TOC content varies between 1.10% and 16.70% and averages at 5.43% (Table 1). All the samples showed good hydrocarbon potential.

4.1.3. Thermal Maturity

Organic maturity can reflect the hydrocarbon generation stage and type of kerogen, which can be determined by vitrinite reflectance. Hydrocarbon content and the state generated by organic matter in different mature stages have significant differences. According to the different types of organic-matter gas-generation modes, type III kerogen directly enters the gas-generation stage when the R_o reaches 0.5% [22]. The testing results from the Longtan Shale samples indicate that the thermal maturity is low as it ranges from 0.736% to 1.06% and averages at 0.923% (Table 1). Its evolution stage is mature and at the peak of gas generation.

Table 1. The Longtan Shale mineral composition in western Guizhou.

Well	Sample ID	Depth (m)	Formation	TOC (%)	R_O (%)	Macerals					Mineral Composition (%)			Clay Composition (%)			
						Sapropelinite	Exinite	Vitrinite	Inertinite	Kerogen Type	Brittle	Carbonate	Clay	I/S	I	K	C
HP 3	HP 3 S1	894.07	P_2l	3.22	0.902	7	10	73	10	III	36.30	0	63.70	46.00	2.00	35.00	17.00
HP 3	HP 3 S2	940.45	P_2l	3.79	1.060	23	35	34	8	II_2	25.10	0	74.90	43.00	2.00	31.00	24.00
HP 3	HP 3 S3	962.15	P_2l	6.05	1.024	9	13	51	27	III	38.80	6.10	55.10	62.00	4.00	22.00	12.00
HP 3	HP 3 S4	980.15	P_2l	8.69	0.918	25	34	33	8	II_2	44.10	0	55.90	2.00	1.00	62.00	35.00
HP 3	HP 3 S5	1009.03	P_2l	1.10	0.986	14	10	65	11	III	21.60	1.20	77.20	62.00	2.00	21.00	15.00
YL 4	YL 4 S1	344.88	P_2l	13.70	0.757	13	40	40	7	III	59.60	0.60	39.80	2.00	2.00	49.00	47.00
YL 4	YL 4 S2	346.80	P_2l	1.83	0.736	8	19	70	3	III	30.40	1.40	68.20	26.00	1.00	33.00	40.00
YL 4	YL 4 S3	357.87	P_2l	16.70	0.890	6	16	71	7	III	65.00	25.70	9.30	2.00	2.00	19.00	77.00
YL 4	YL 4 S4	403.71	P_2l	2.46	0.820	14	41	42	3	II_2	45.50	3.90	50.60	20.00	2.00	41.00	37.00
YL 4	YL 4 S5	428.76	P_2l	2.43	0.821	2	11	75	12	III	39.00	12.00	49.00	50.00	5.00	14.00	31.00
YL 4	YL 4 S6	452.46	P_2l	2.65	0.914	2	9	74	15	III	34.30	0.30	65.40	74.00	3.00	12.00	11.00
YL 4	YL 4 S7	488.19	P_2l	3.60	0.920	3	12	75	10	III	27.10	9.90	63.00	78.00	4.00	9.00	9.00
YL 4	YL 4 S8	522.68	P_2l	4.85	0.960	15	46	27	12	II_2	24.90	0.40	74.70	58.00	2.00	24.00	16.00
YL 4	YL 4 S9	548.06	P_2l	8.27	0.961	2	5	89	4	III	30.60	0	69.40	72.00	3.00	14.00	11.00
YL 4	YL 4 S10	561.12	P_2l	3.22	0.961	3	13	77	7	III	39.10	0	60.90	49.00	2.00	16.00	33.00
YL 4	YL 4 S11	573.69	P_2l	4.67	0.966	2	5	81	12	III	41.80	0	58.20	57.00	1.00	22.00	20.00
YL 4	YL 4 S12	585.12	P_2l	7.03	0.975	17	41	32	10	II_2	33.70	0.70	65.60	60.00	2.00	20.00	18.00
YL 4	YL 4 S13	588.98	P_2l	6.69	0.939	2	7	87	4	III	42.20	3.20	54.60	43.00	1.00	25.00	31.00
YL 4	YL 4 S14	612.52	P_2l	2.17	1.023	2	15	63	20	III	21.60	0	78.40	2.00	2.00	49.00	47.00
Average	/	/	/	5.43	0.923	7	10	73	10	III	36.88	3.44	59.68	42.53	2.26	27.26	27.95

4.2. Mineral Composition

The shale mineral composition is rich, and the brittle mineral content greatly affects the fracture generation ability in shale reservoirs. Therefore, the study of mineral composition is particularly important. The Longtan Shale minerals mostly consist of clay minerals (kaolinite, chlorite, illite, and illite–smectite mixed layer), brittle minerals (quartz, feldspar, siderite, and pyrite), and carbonate minerals (calcite and dolomite) (Table 1 and Figure 2). The clay minerals have the highest concentration of 59.68%, ranging from 9.30% to 78.40%. The porosity and microfractures are large, and the pore distribution characteristics are complex when the clay mineral content is high, which leads to a good gas-adsorption capacity. The brittle mineral content is relatively high, ranging between 21.60% and 65.00%, with a mean of 36.88%, which means it is profitable for shale fracturing. The carbonate mineral content ranges between 0% and 25.70% and averages at 3.44% (Table 1).

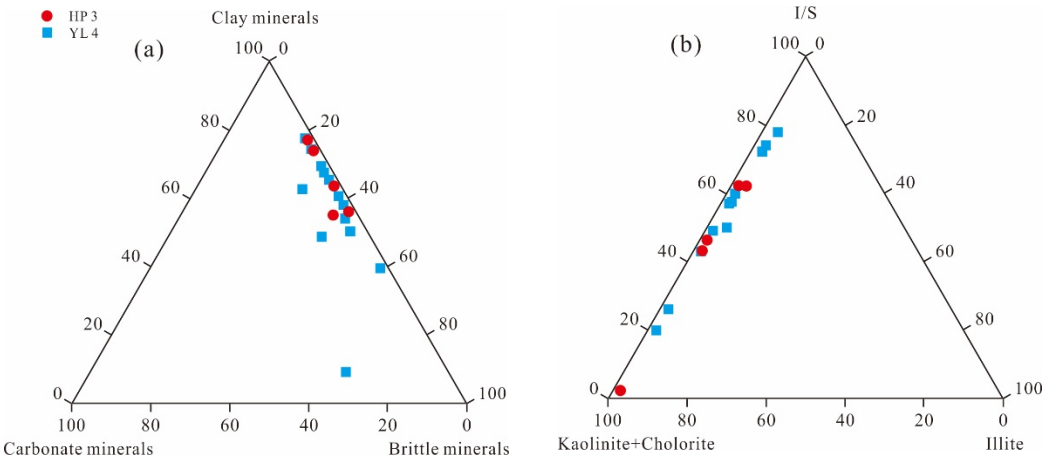

Figure 2. The Longtan Shale mineral distribution: (**a**) triangle diagram of the mineral distribution and (**b**) triangle diagram of the clay mineral distribution. I/S = illite–smectite mixed layer.

The clay minerals consist of illite, illite–smectite mixed layer, and other minerals such as kaolinite and chlorite. The other minerals' content, such as kaolinite and chlorite, is the highest, ranging from 18.00% to 97.00%, with a mean of 55.21%. The illite–smectite mixed layer content ranges between 2.00% and 78.00% and averages at 42.53%. The illite content ranges between 1.00% and 5.00% and averages at 2.26% (Table 1). The high illite–smectite mixed layer content reflects the sedimentary environment, which, at that time, was an oxygen-deficient and relatively reductive environment. It is profitable for organic matter preservation and enrichment, and it provides a suitable environment for hydrocarbon gas generation and enrichment.

4.3. Types of Shale Pores

According to the shale pore structural characteristics and genesis, the Longtan Shale reservoir space consists of intergranular pores, intragranular pores, organic pores, and microfractures (Table 2), and this was determined based on the SLATT method and the O'Brien six-division method of shale pore types [23].

Table 2. The Longtan Shale pore type classification in western Guizhou [23–25].

Pore Types	Genetic Mechanism	Location	Morphological	Pore Diameter
Intergranular pores	Primary sedimentary, cementation, diagenesis	Between clay mineral particles	Silt, layered	50 nm–1 μm
		Between brittle mineral particles, between plastic minerals and brittle mineral particles, between organic matter blocks and brittle minerals	Irregular, ink bottle	100 nm–1 μm
Intragranular pores	Postdiagenesis	Between pyrite crystals	Elliptical, nearly circular, ink bottle	20 nm–500 nm
		Dissolution of soluble minerals	Elliptical, irregular	20 nm–1 μm
Organic pores	Hydrocarbon generation evolution of organic matter	Internal pores of organic matter	Elliptical, bubble-like, irregular polygonal	5 nm–300 nm
Microfractures	Stress effect	Tectonic fractures	Elongated	20 nm–300 nm

4.3.1. Intergranular Pores

Intergranular pores refer to the pores that are supported by brittle mineral particles and which are not filled in particles. Intergranular pores mainly exist between clay mineral floccules or between mineral particles. Clay-mineral-related intergranular pores develop well in the Longtan Shale, which are of the ink-bottle (Figure 3b) and layered (Figure 3a,b) types. The pore diameter ranges between 50 nm and 1 μm. When the clay minerals and brittle minerals are randomly distributed, the clay-mineral-related intergranular pores are usually well preserved because of the support of the brittle mineral. In addition, microfractures are formed within the brittle minerals. Those in contact with plastic clay minerals communicate with clay-mineral-related intergranular pores; therefore, the intergranular pores connectivity was found to be good. The pores between brittle minerals (Figure 3a,g), the pores between plastic mineral particles and brittle mineral particles (Figure 3b), and the intergranular pores between organic matter block edges and mineral particles (Figure 3e) were observed under SEM. They had mostly irregular shapes, with pore diameters varying between 100 nm and 1 μm. Intergranular pores have good internal connectivity and are an important migration channel for shale gas.

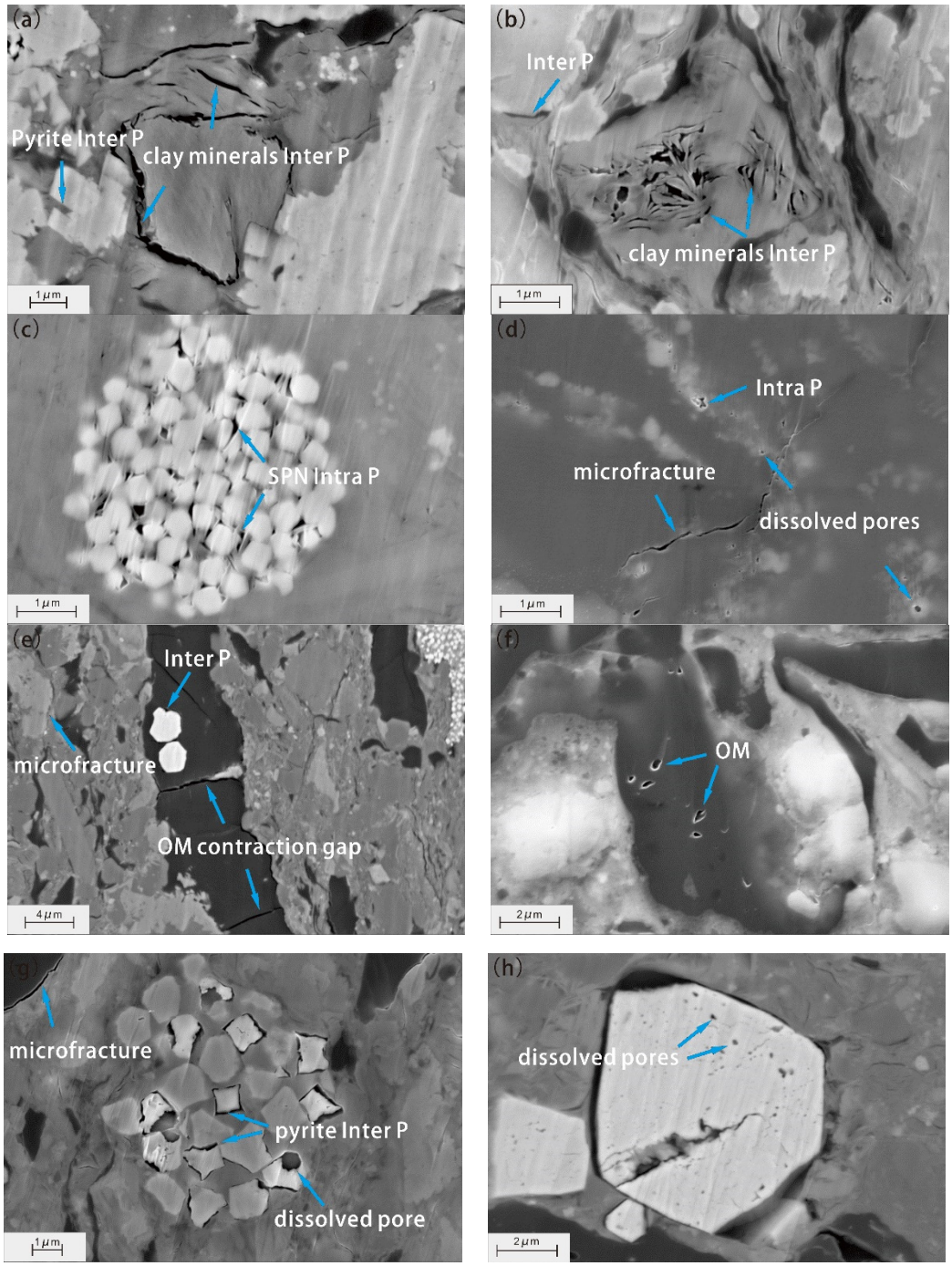

Figure 3. The Longtan Shale pore types and characteristics. SPN = strawberry pyrite nodules; Inter P = intergranular pores; Intra P = intragranular pores; OM = organic matter. (**a**) YL 4 well, 522.68 m; (**b**) YL 4 well, 588.98 m; (**c**) HP 3 well, 894.07 m; (**d**) HP 3 well, 1009.03 m; (**e**) YL 4 well, 403.71 m; (**f**) YL 4 well, 612.52 m; (**g**) YL 4 well, 403.71 m; and (**h**) YL 4 well, 561.12 m.

4.3.2. Intragranular Pores

Intragranular pores are generally formed inside mineral particles, with irregular pore morphology. Strawberry pyrite nodules are relatively common in organic-rich shale. They are formed of numerous small pyrite crystals. There are micropores among these crystals (Figure 3c), which have a pore diameter range of 20 nm to 500 nm. During the diagenesis process, the dissolution of minerals can generate dissolution pores [24] (Figure 3d,g,h), which are mostly elliptical and irregular in shape, albeit with smooth edges. The pore diameter varies between 20 nm and 1 μm, and it is susceptible to compaction.

4.3.3. Organic Pores

The thermal degradation of kerogen toward oil and gas can produce secondary pores and carbon-rich residues during the mature to over-matured stages. When the R_o reaches 0.6% or above, organic pores begin to develop [10,25]. The Longtan Shale R_o is greater than 0.7% (Table 1), which is sufficient for developing organic pores. However, small numbers of organic pores could be observed under a microscope (which is only occasionally seen in a few types of organic matter), and the pore diameter varied between 5 nm and 300 nm. Different from the spongy organic pores found in high- and over-high-mature marine shales, the organic pores that had developed in type III kerogen were mostly bubble-like (Figure 3f), and this may have been caused by the different hydrocarbon generation behaviors of the organic matter [26]. Not all kerogen types are easy-to-form organic pores. Type III kerogen is a type of solid organic matter with a macromolecular cross-linked structure in comparison to type I and II kerogen. Their thermal degradation is a process of "defunctionalization". In this process, it is hard to form organic pores if the macromolecular structure is not depolymerized [27].

4.3.4. Microfractures

A great number of microfractures are formed during the diagenesis process and later the transformation process. Furthermore, microfractures also form at the edge of the organic matter in the hydrocarbon generation process (Figure 3g). These abundant microfractures can provide migration channels for oil and gas, which is beneficial for later transformation. Microfractures in shale are often found between mineral particles (Figure 3e) or between mineral particles and organic matter (Figure 3g). They are usually caused by clay-mineral or organic-matter volume reduction, as well as by uneven internal stress within organic matter [28] (Figure 3d,e). Due to the frequent tectonic activity in western Guizhou, a large number of microfractures with nanoscale width and micro–nanoscale length can be observed under a microscope, most of which are elongated in shape (Figure 3d). Moreover, the brittle mineral content is a significant influence factor for shale porosity, microfracture development degree, gas-bearing capacity, and fracturing treatment methods. The Longtan Shale brittle mineral content is comparatively high, and it averages at 36%, which is more likely to generate fractures and increase the resistance to mechanical compaction. However, it is profitable for primary pore preservation.

4.4. Pore Morphology and Structure Characteristics

Isotherm adsorption curves that are obtained from low-temperature nitrogen adsorption experiments contain information about pore structure and pore type. In 1985, IUPAC introduced the capillary condensation phenomenon and proposed to divide the isothermal adsorption curves of gases into six basic types [29]. In 2015, IUPAC supplemented and improved the scheme proposed in 1985 [30] (Figure 4). The isotherm adsorption curves of the Longtan Shale are mainly IV(a) isotherm (Figure 5) with an inverse "S" shape. This shows that the adsorbent gas undergoes capillary condensation, and that the adsorption curve increases rapidly after reaching a certain pressure. The hysteresis loop is formed due to non-coincidence between the desorption curve and the adsorption curve. It also indicates that the samples are mainly composed of mesoporous pores.

The structure characteristics of the shale pores can be judged based on the morphology of the hysteresis loops on the nitrogen adsorption–desorption curves [31,32]. Various scholars have proposed a number of pore structure classification schemes based on hysteresis loop morphology. According to the differences in hysteresis loop morphology and pore structure, Sing (1985) [29] summarized four types of curves based on the classification of de Boer (1958) [33] and combined pore structure and hysteresis loop morphology; different hysteresis loops correspond to specific pore types (Figure 6). All samples from the Longtan Shale exhibited desorption hysteresis, thereby forming hysteresis loops with the adsorption branches, which means that capillary condensation occurred in the mesoporous samples [29]. According to the desorption hysteresis types (Figure 6), the morphological

characteristics of the hysteresis loops in the HP 3 well and YL 4 well belong to type H_2. The interval between the adsorption and desorption curves of the hysteresis loops was relatively large, and the desorption curves showed a feature of rapid decline after reaching a certain relative pressure point. The pores were mainly of the ink-bottle shape with a thin neck and wide body, which act as the "bottleneck" of the ink-bottle type. Most of these pores are clay-mineral-related intergranular pores (Figure 3b). Different from the HP 3 well, some of the hysteresis loops of shale samples in the YL 4 well belong to type H_3. These hysteresis loops show a characteristic of not reaching saturation adsorption in high-pressure zones, which are mainly characterized by slit pores and layered pores (Figure 3a,b). It is noteworthy that most shale samples from the HP 3 well and YL 4 well had unclosed hysteresis loops at low relative pressures, which may be due to the expansion of shale or organic matter during adsorption, incomplete desorption of nitrogen, or the irreversible absorption in pores with similar diameters to nitrogen molecules [15,34].

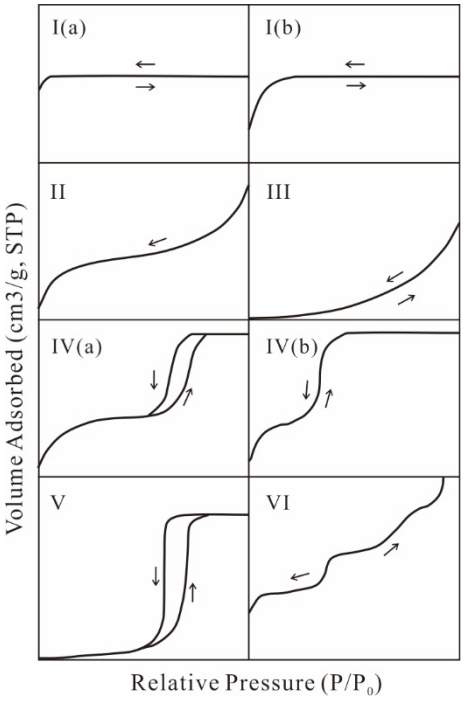

Figure 4. Classification of the IUPAC adsorption isotherm (according to Thommes et al., 2015 [30]).

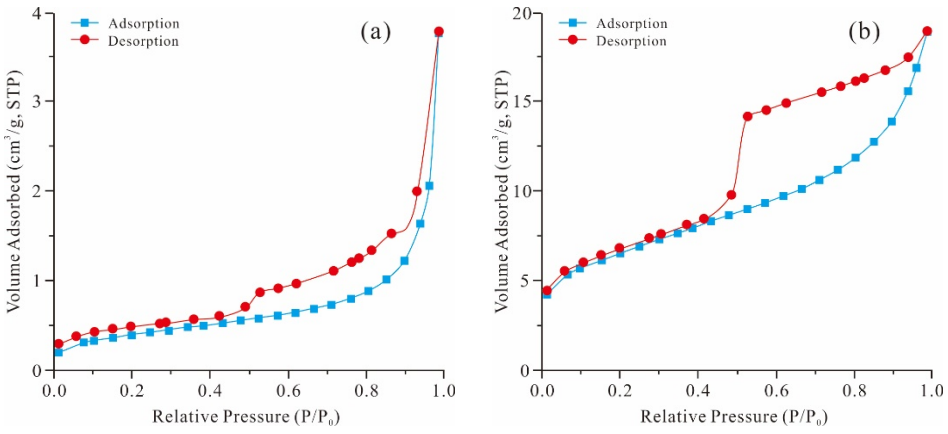

Figure 5. *Cont.*

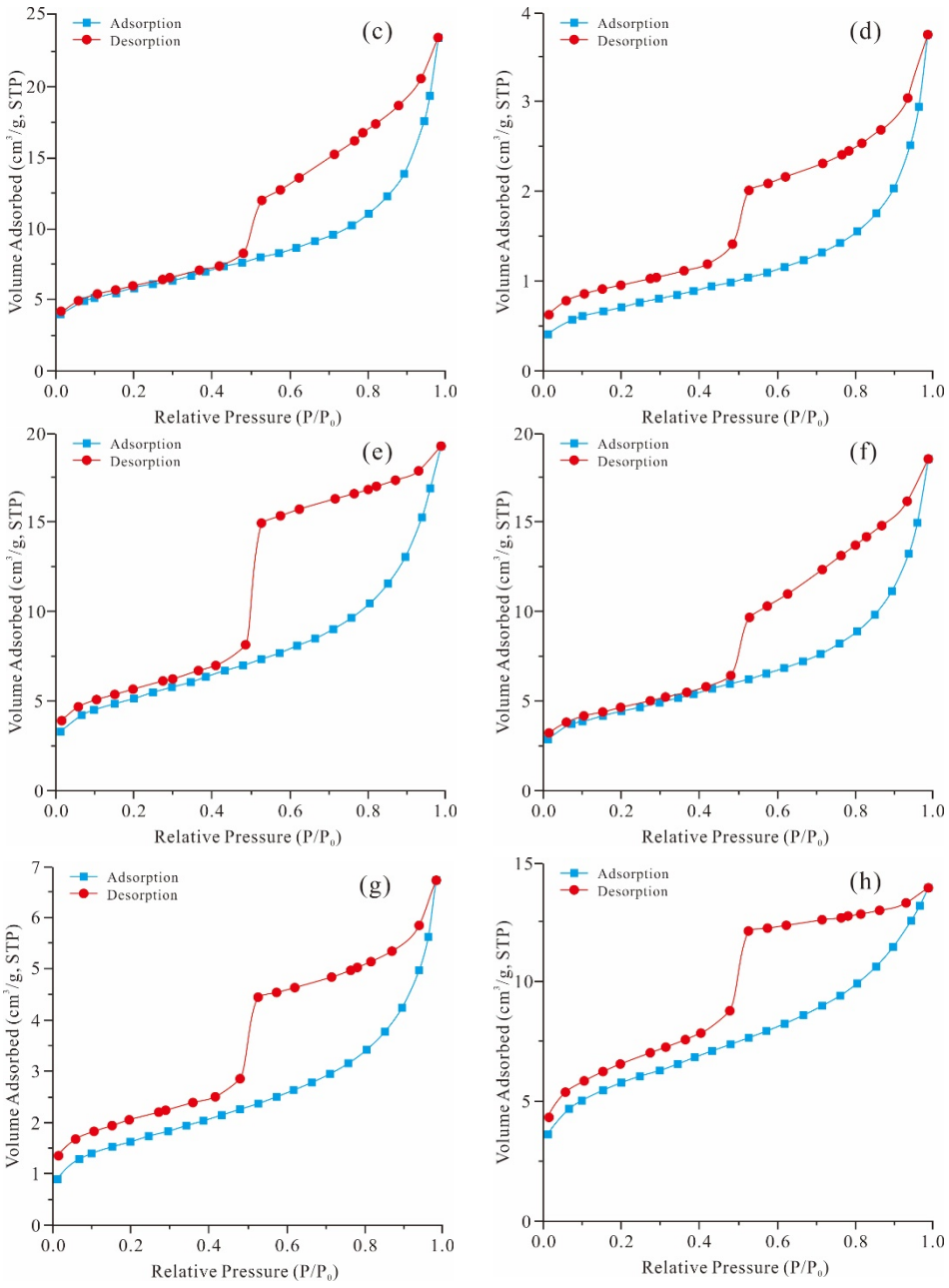

Figure 5. Isotherm adsorption curves of the Longtan Shale in western Guizhou. (**a**) YL 4 well, 357.87 m; (**b**) YL 4 well, 403.71 m; (**c**) YL 4 well, 488.19 m; (**d**) YL 4 well, 573.69 m; (**e**) HP 3 well, 940.45 m; (**f**) HP 3 well, 962.15 m; (**g**) HP 3 well, 980.15 m; and (**h**) HP 3 well, 1009.03 m.

Nitrogen adsorption can be used to characterize pore diameter distribution by differential pore volumes, logarithmic integral pore volumes, the cumulative adsorption amount, and stage adsorption increments [35]. Among them, the differential pore volume can indicate the reservoir space concentration degree in different pore diameter ranges. In this research, the DFT model was applied to describe the shale pore diameter distribution. The pore diameter distribution curves of the Longtan Shale samples all showed multi-peak characteristics (Figure 7), indicating a complex pore structure and a large-scale range in the pore diameter. The main peaks of the HP 3 well samples were concentrated at the 9 nm, 20 nm, and 40 nm range, with the peaks varying from 0.011 cm^3/g to 0.016 cm^3/g. Other peaks appeared at the 1.5 nm, 2 nm, and 4 nm range, with peaks varying between 0.005 cm^3/g and 0.011 cm^3/g. This indicated that the shale samples mostly developed mesopores, followed by micropores. The main peaks of the YL 4 well samples were concen-

trated at the 20 nm, 40 nm, and 50 nm range, and the peaks varied between 0.0026 cm^3/g and 0.023 cm^3/g. Other peaks appeared at the 1.5 nm, 9 nm, and 70 nm range, with peaks varying from 0.0008 cm^3/g to 0.014 cm^3/g. This showed that the shale samples mostly developed mesopores, followed by macropores.

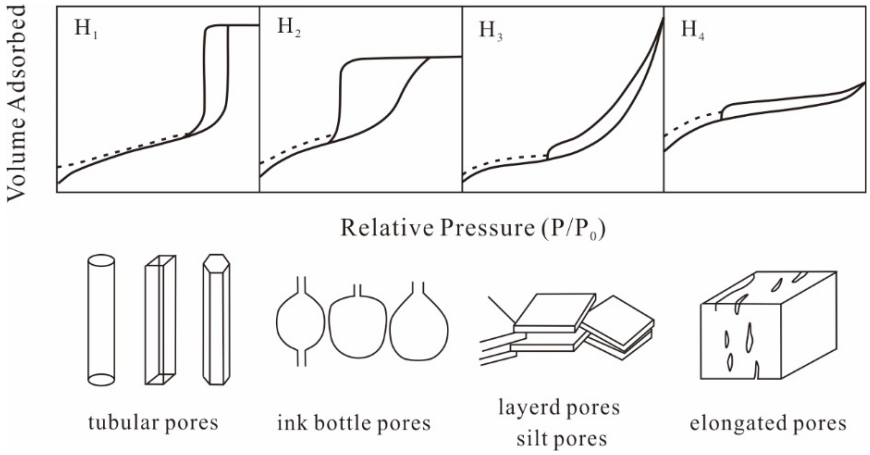

Figure 6. IUPAC hysteresis loop classification [29].

4.5. Pore Volumes and the SSA

The Brunauer–Emmett–Teller (BET) model was used to calculate the pore volume and the SSA [36] (Table 3). The pore volume of the Longtan Shale samples from the HP 3 well ranged between 0.007797 cm^3/g and 0.029955 cm^3/g, averaging at 0.019408 cm^3/g. The SSA varied between 2.90 m^2/g and 20.50 m^2/g, with averages at 12.65 m^2/g. The average pore diameter ranges were between 4.28 nm and 10.40 nm, with averages at 7.21 nm. The pore volume of the YL 4 well shale samples varied between 0.005438 cm^3/g and 0.036434 cm^3/g, averaging at 0.022314 cm^3/g. The SSA varied between 1.20 m^2/g and 27.80 m^2/g, averaging at 14.48 m^2/g. The average pore diameter varied between 4.81 nm and 18.10 nm, with averages at 8.15 nm. By comparison, the pore volume, the SSA, and the average pore diameter of the YL 4 well shale samples were slightly higher than those from the HP 3 well. The Longtan Shale SSA was provided primarily by the pores with a pore diameter varying from 5 nm to 10 nm. The numerous nanoscale pores in the Longtan Formation can greatly increase the SSA and offer plenty of space for shale gas occurrence.

The Longtan Shale total pore volume in western Guizhou varies between 0.005438 cm^3/g and 0.036434 cm^3/g, with averages at 0.021549 cm^3/g. The mesopores (2 nm < Φ < 50 nm) occupy most of the pore volume, varying from 0.002588 cm^3/g to 0.030858 cm^3/g with a mean of 0.017339 cm^3/g. The macropore volume (Φ > 50 nm) ranges between 0.001306 cm^3/g and 0.008306 cm^3/g, with averages at 0.003484 cm^3/g. The micropore volume accounts for a small portion of the total pore volume, varying from 0.000068 cm^3/g to 0.001604 cm^3/g, with a mean of 0.000727 cm^3/g (Table 3). These results indicate that mesopores contribute the most to the Longtan Shale pore volume in western Guizhou, followed by macropores and micropores.

The Longtan Shale SSA was positively correlated with pore volume (Figure 8), indicating that the shale SSA increases along with pore volume. The negative correlation between the average pore diameter and the SSA (Figure 9) indicated that a smaller pore diameter accounts for a larger proportion in the SSA.

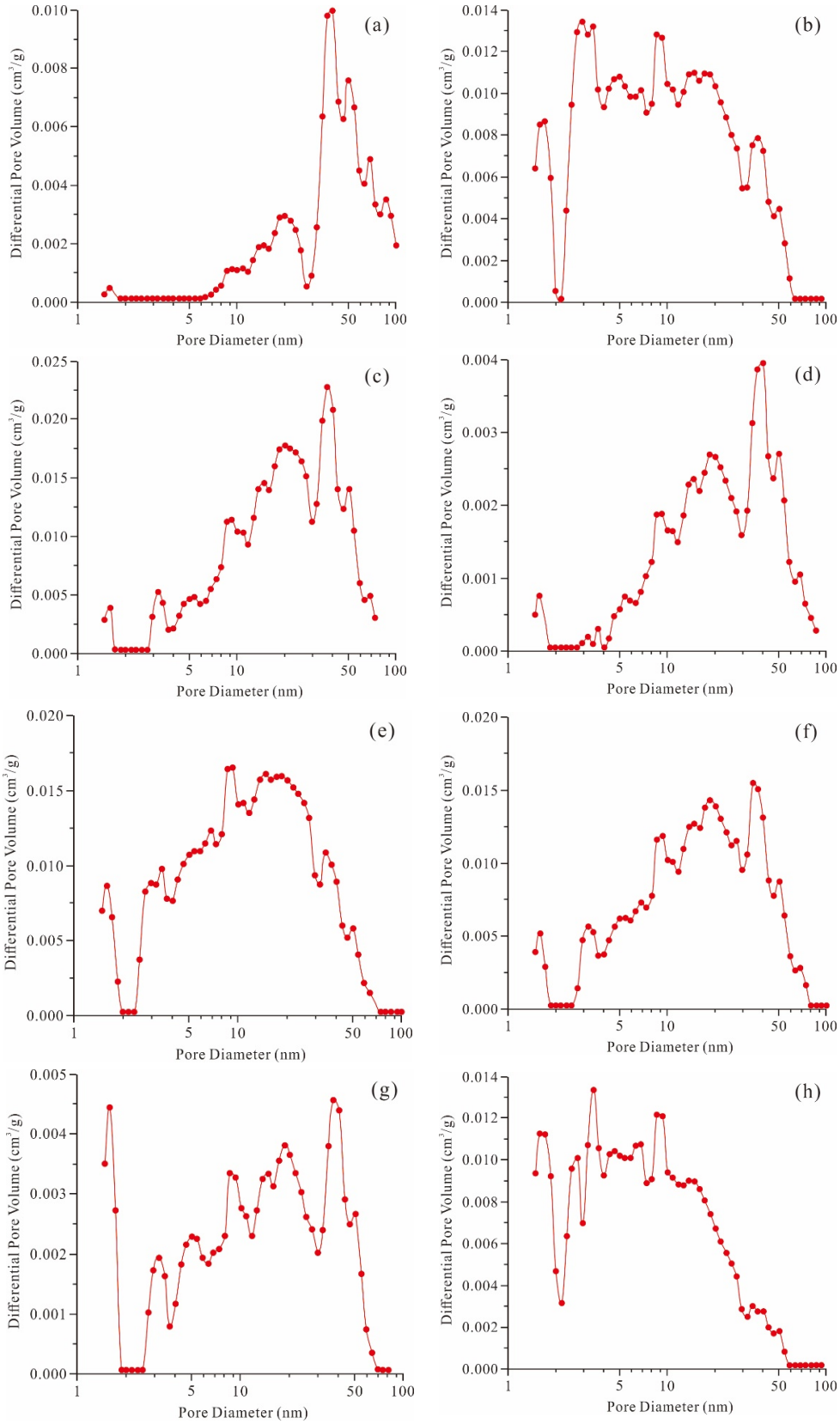

Figure 7. The Longtan Shale pore volume and pore diameter in western Guizhou. (**a**) YL 4 well, 357.87 m; (**b**) YL 4 well, 403.71 m; (**c**) YL 4 well, 488.19 m; (**d**) YL 4 well, 573.69 m; (**e**) HP 3 well, 940.45 m; (**f**) HP 3 well, 962.15 m; (**g**) HP 3 well, 980.15 m; and (**h**) HP 3 well, 1009.03 m.

Table 3. The Longtan Shale pore structure parameters in western Guizhou.

Sample ID	Depth (m)	TOC (%)	R_o (%)	Average Pore Diameter (nm)	Pore Volume (cm^3/g)	Micropore Volume (cm^3/g)	Mesopore Volume (cm^3/g)	Macropore Volume (cm^3/g)	S_{BET} (m^2/g)
HP 3 S1	894.07	3.22	0.902	10.40	0.007797	0.000109	0.006043	0.001645	2.90
HP 3 S2	940.45	3.79	1.060	6.61	0.029955	0.000878	0.024931	0.004146	18.40
HP 3 S3	962.15	6.05	1.024	7.43	0.028353	0.000597	0.021557	0.006199	15.60
HP 3 S4	980.15	8.69	0.918	7.31	0.010682	0.000304	0.008463	0.001915	5.83
HP 3 S5	1009.03	1.10	0.986	4.28	0.020251	0.001344	0.017601	0.001306	20.50
YL 4 S1	344.88	13.70	0.757	18.10	0.005438	0.000068	0.002588	0.002782	1.20
YL 4 S2	346.80	1.83	0.736	5.37	0.036434	0.001561	0.030858	0.004015	27.80
YL 4 S3	357.87	16.70	0.890	16.90	0.006054	0.000088	0.00294	0.003026	1.43
YL 4 S4	403.71	2.46	0.820	5.13	0.028421	0.001372	0.023543	0.003506	23.00
YL 4 S5	428.76	2.43	0.821	5.42	0.018027	0.000729	0.015253	0.002045	13.80
YL 4 S6	452.46	2.65	0.914	6.95	0.035502	0.000856	0.02634	0.008306	21.40
YL 4 S7	488.19	3.60	0.920	7.16	0.03539	0.000781	0.027435	0.007174	20.50
YL 4 S8	522.68	4.85	0.960	7.66	0.031765	0.000742	0.02535	0.005673	16.60
YL 4 S9	548.06	8.27	0.961	6.57	0.023904	0.000814	0.020611	0.002479	14.50
YL 4 S10	561.12	3.22	0.961	4.81	0.029846	0.001604	0.025878	0.002364	26.00
YL 4 S11	573.69	4.67	0.966	9.34	0.0059	0.000078	0.004417	0.001405	2.53
YL 4 S12	585.12	7.03	0.975	7.54	0.025585	0.000763	0.02043	0.004392	13.60
YL 4 S13	588.98	6.69	0.939	7.99	0.012952	0.0003	0.01042	0.002232	6.34
YL 4 S14	612.52	2.17	1.023	5.10	0.017182	0.000816	0.014784	0.001582	14.00
Average	/	5.43	0.923	7.90	0.021549	0.000727	0.017339	0.003484	14.00

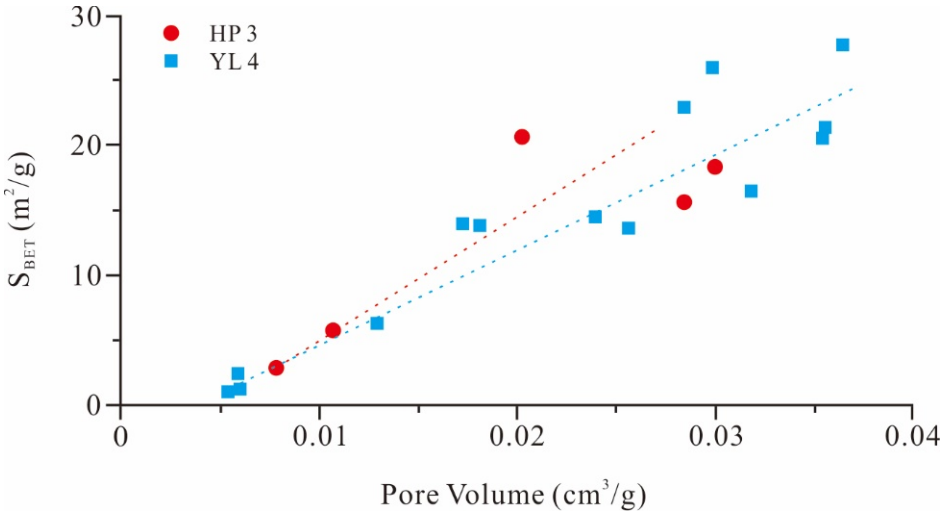

Figure 8. Relationship between pore volume and the SSA.

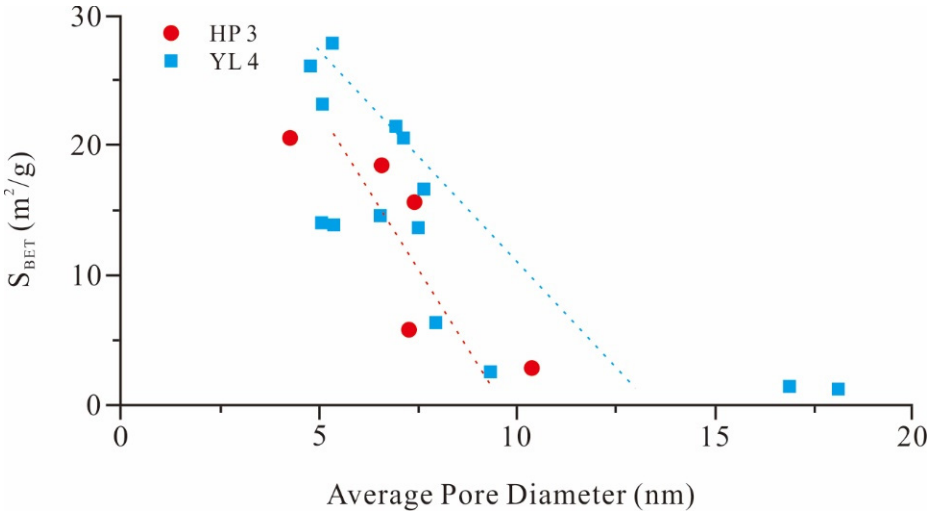

Figure 9. Relationship between the average pore diameter and the SSA.

5. Discussion

5.1. The Influence of Mineral Composition on Pore Development

5.1.1. Relationship between Pore Structure Characteristics and Brittle Minerals

As the supporting minerals in shales, brittle minerals can effectively bear the pressure in diagenesis. However, the brittle mineral content is found to be negatively correlated with the Longtan Shale pore parameters in western Guizhou (Figure 10), indicating that the brittle minerals' content in this area is not conducive to pore development. There is a large amount of terrigenous injection with high quartz and clay mineral content in the Longtan Shale. It is detrimental to quartz framework network development, as well as to organic-matter injection and preservation, thus resulting in the rare development of micropores around brittle minerals. Although brittle minerals have a certain protection on the macropores and mesopores in the periphery of mineral particles, there are a few pores inside brittle minerals, and these are mainly intergranular pores that are formed between brittle mineral particles. The distribution density of these pores is relatively weak. Therefore, there is a negative relationship between brittle mineral content and micropore volume, mesopore volume, macropore volume, and total pore volume. Moreover, the surface area morphology of brittle minerals (e.g., calcite and quartz) related to pores is simple; in addition, it cannot provide adsorption points, and it contributes little to the SSA.

It is a remarkable fact that strawberry pyrite is common in the Longtan Shale, as determined under SEM. The strawberry pyrite is formed in early diagenesis, and it lacks variation in the later diagenetic process, which can represent the earliest shale diagenetic environment. The high feldspar and clay mineral content of the Longtan Shale provides a large number of iron ions, which provides the main growth conditions for strawberry pyrite. According to the correlation between pyrite and reservoir parameters, each pore structure parameter decreases with increasing pyrite content (Figure 11). On the one hand, it shows that the primary reservoir spaces are not pyrite-related inorganic pores, such as pyrite intergranular pores. On the other hand, the euhedral pyrite formed by sulfate reduction in the closed diagenetic stage and overpressure environment occurs in a large amount of plant-residual structural pores. This metasomatizes clay minerals, which compresses the occurrence space of clay mineral pores and is adverse to pore development.

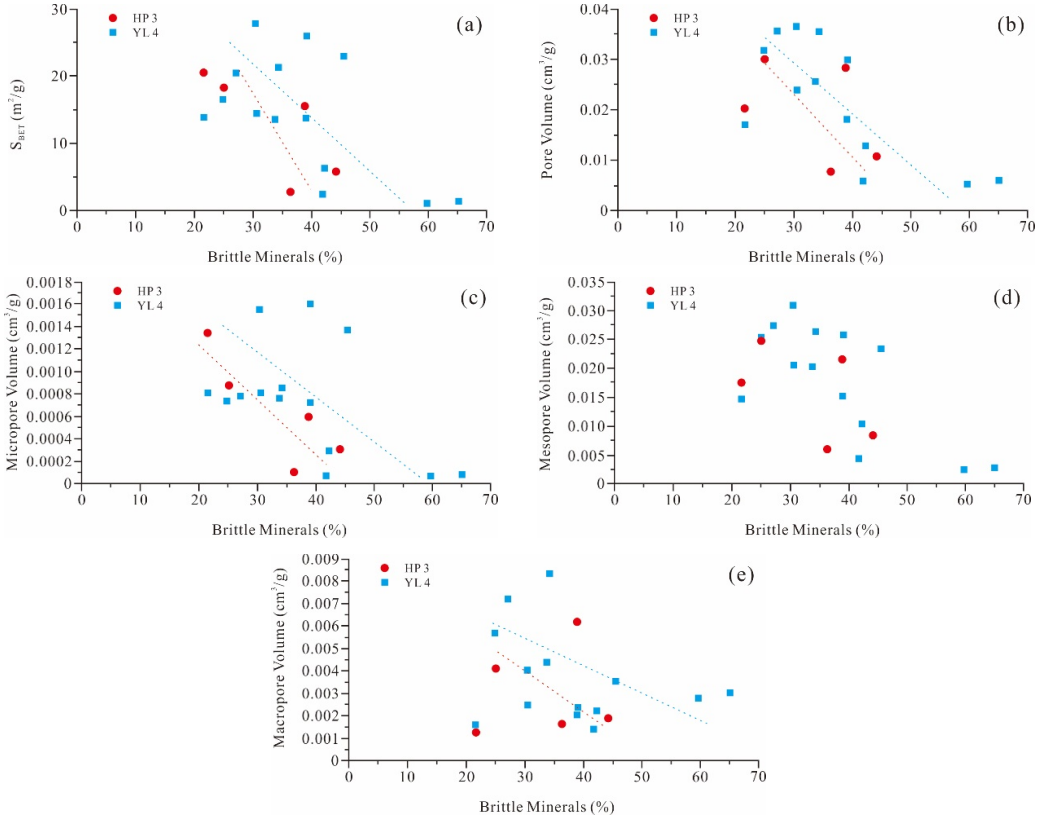

Figure 10. Relationship between pore structure characteristics and brittle minerals.

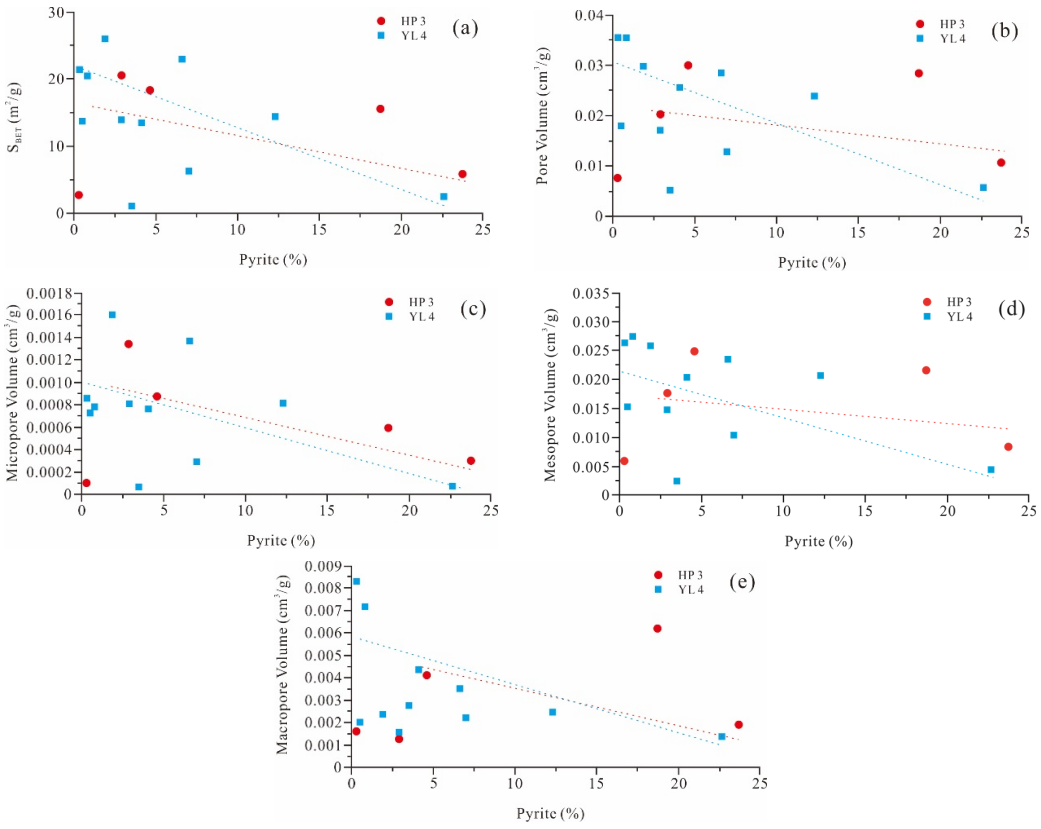

Figure 11. Relationship between pore structure characteristics and pyrite.

5.1.2. Relationship between Pore Structure Characteristics and Carbonate Minerals

The low carbonate mineral content in the Longtan Shale ranges between 0% and 25.70%, with averages at 3.44%. The bedding microfractures and shrinkage microfractures are well-developed, while the dissolution microfractures are rare. Carbonate minerals are soluble minerals that can form secondary dissolution pores under acidic fluids. Most of the secondary dissolution pores exist in isolated point shapes with a small amount of pores, and they do not have reservoir significance. Moreover, carbonate minerals are prone to chemical cementation, thereby forming secondary calcite, enlarging iron dolomite ring edges (achieved by filling in the primary pores or fractures in the form of calcite), or blocking intergranular pores. Consequently, each pore structure parameter is negatively correlated to the carbonate mineral content (Figure 12).

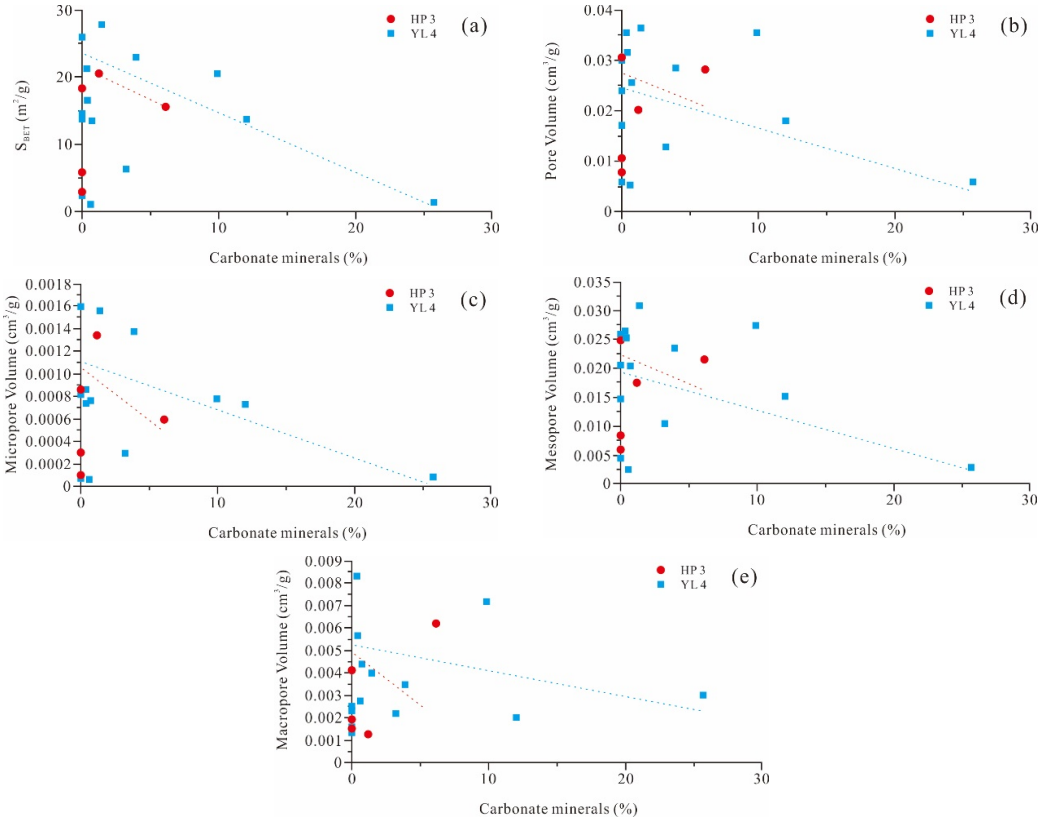

Figure 12. Relationship between pore structure characteristics and carbonate minerals.

5.1.3. Relationship between Pore Structure Characteristics and Clay Minerals

The clay mineral content in the Longtan Shale varies from 9.30% to 78.40%, with averages at 59.68%. The high clay mineral content forms the material foundation of clay-mineral-related pores. Due to the rich content of type III kerogen in the Longtan Shale, it can protect clay-mineral-related pores from the influence of organic matter injection, thus making it the main pore type of this formation. As shown in Figure 13, a positive correlation was found between the clay mineral content and micropore volume, mesopore volume, total pore volume, and the SSA. This indicates that the contribution of clay minerals to shale pores was mainly reflected in the micropores and mesopores, while the control effect on the macropores was not obvious. In the middle diagenetic period of the Longtan Shale, clay minerals undergo compaction and dehydration during the consolidation process, thus leading to volume shrinkage and the formation of new microfractures. These microfractures have a small extension length, but mostly have good connectivity. It is worth noting that the macropore volume shows a tendency to first increase and then decrease with increasing clay mineral content, indicating that too low or too high clay mineral content is unfavorable

for macropore development. This is because shales with high clay mineral content are prone to compaction and deformation, leading to a sharp decrease in large primary pores. Moreover, high clay mineral content can cause brittleness reduction and a strengthening of the tensile shear ability of shale, which is adverse to structural fracture development.

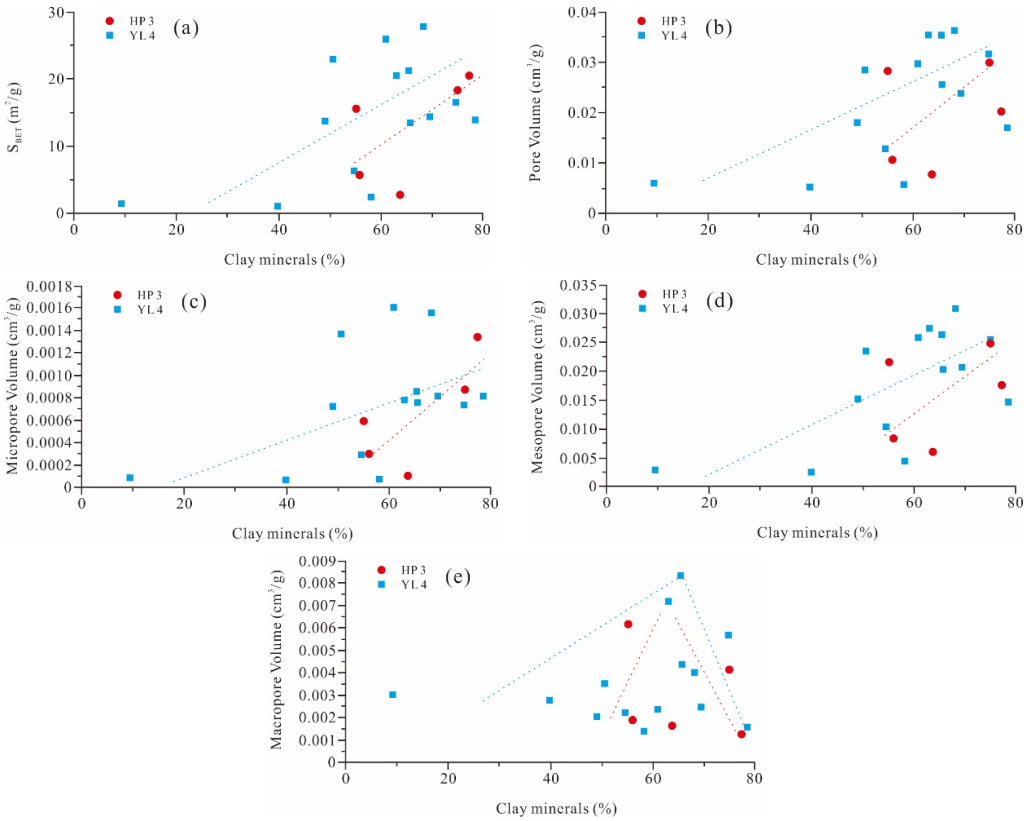

Figure 13. Relationship between pore structure characteristics and clay minerals.

Different clay minerals have great differences in morphology, structure, chemical properties, and physical properties. The effects on shale pore development are also different. X-ray diffraction analysis showed that the Longtan Shale clay minerals consist of illite–smectite mixed layer, chlorite, kaolinite, and slight illite deposits. The Longtan Shale clay minerals do not contain montmorillonite, which indicates that with the increasing depth, along with compaction and dehydration, the increasing temperature and pressure makes montmorillonite gradually transform into illite. In the transitional stage, there is illite–smectite mixed layer. The pores and fractures between clay minerals are the most developed in this stage due to the collapse of montmorillonite.

The pore structure parameters positively correlated with illite–smectite mixed layer content (Figure 14) suggests that illite–smectite mixed layer is profitable for shale pore development. The illite–smectite mixed layer particles have a rough surface, which increases the shale SSA and pore volume, as well as provides more storage and adsorption space for shale gas [37]. The chlorite and kaolinite content negatively correlated with the pore structure parameters (Figures 15 and 16). The negative correlation between the micropore volume and chlorite was found to be significant, which indicated that chlorite has a negative effect on shale pore development, especially on micropore volume. The content of illite was only between 1.00% and 5.00%, with an average of 2.26%, and this was not relative to the pore structure parameters (Figure 17). This indicated that the illite–smectite mixed layer is the main factor controlling clay-mineral-related pores; meanwhile, illite has no obvious control over clay-mineral-related pores and the SSA.

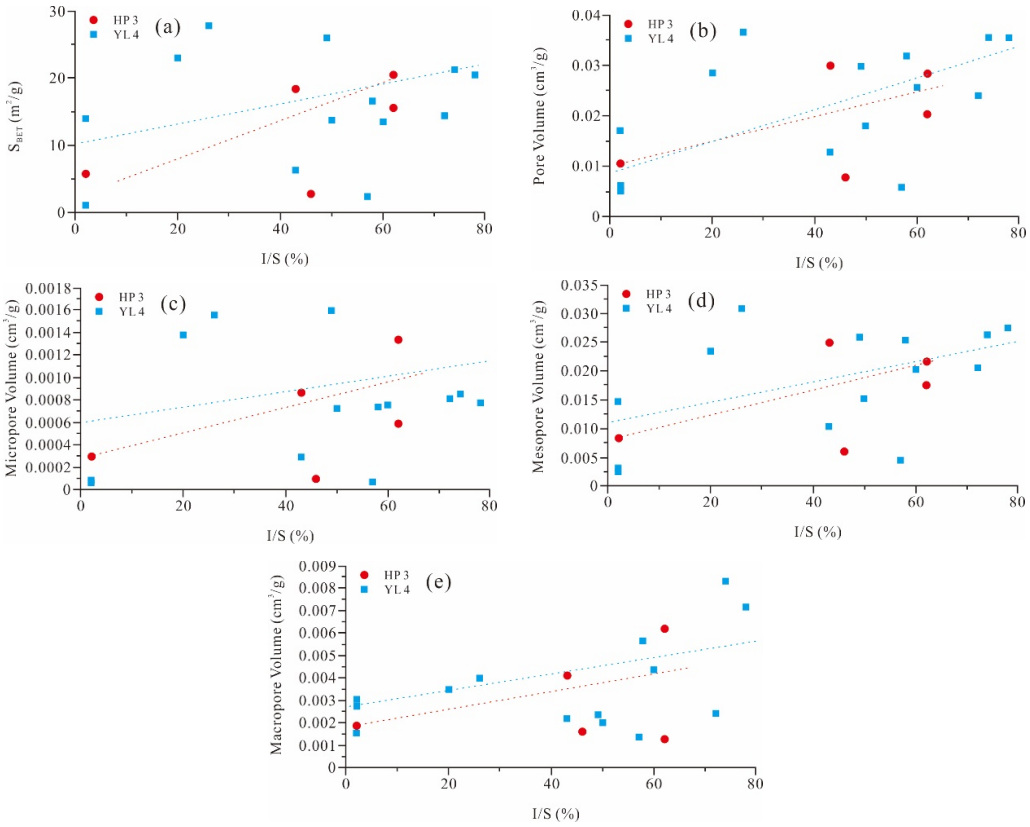

Figure 14. Relationship between pore structure characteristics and I/S.

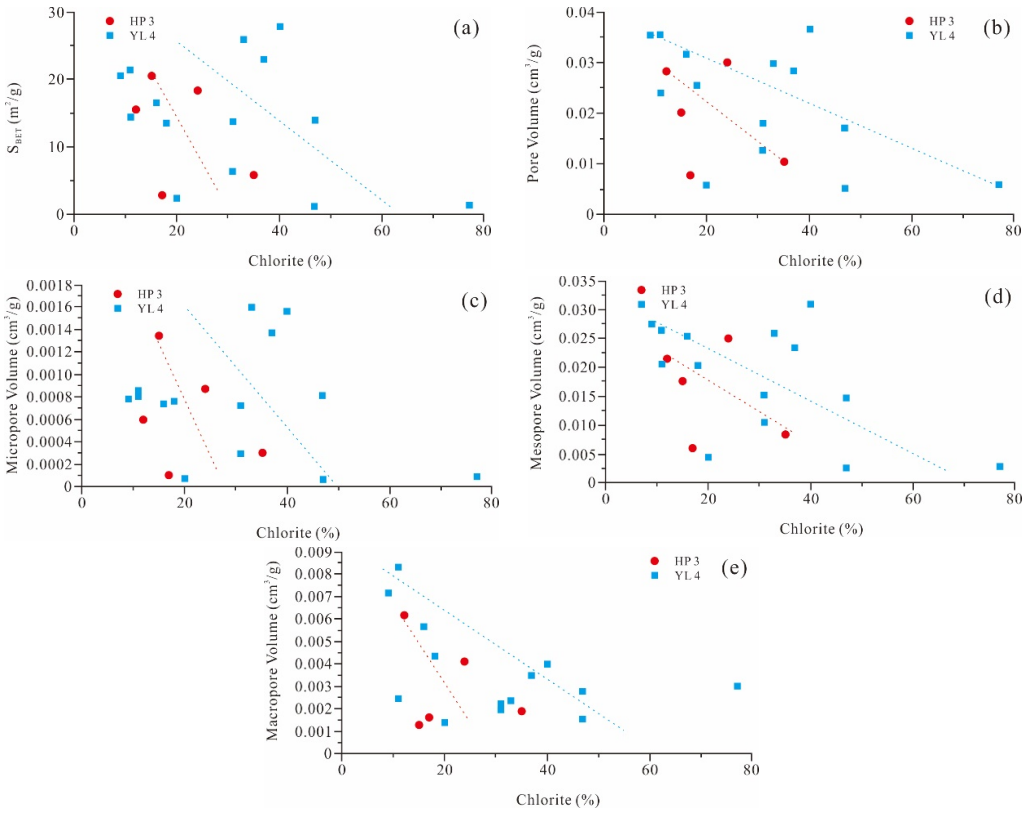

Figure 15. Relationship between pore structure characteristics and chlorite.

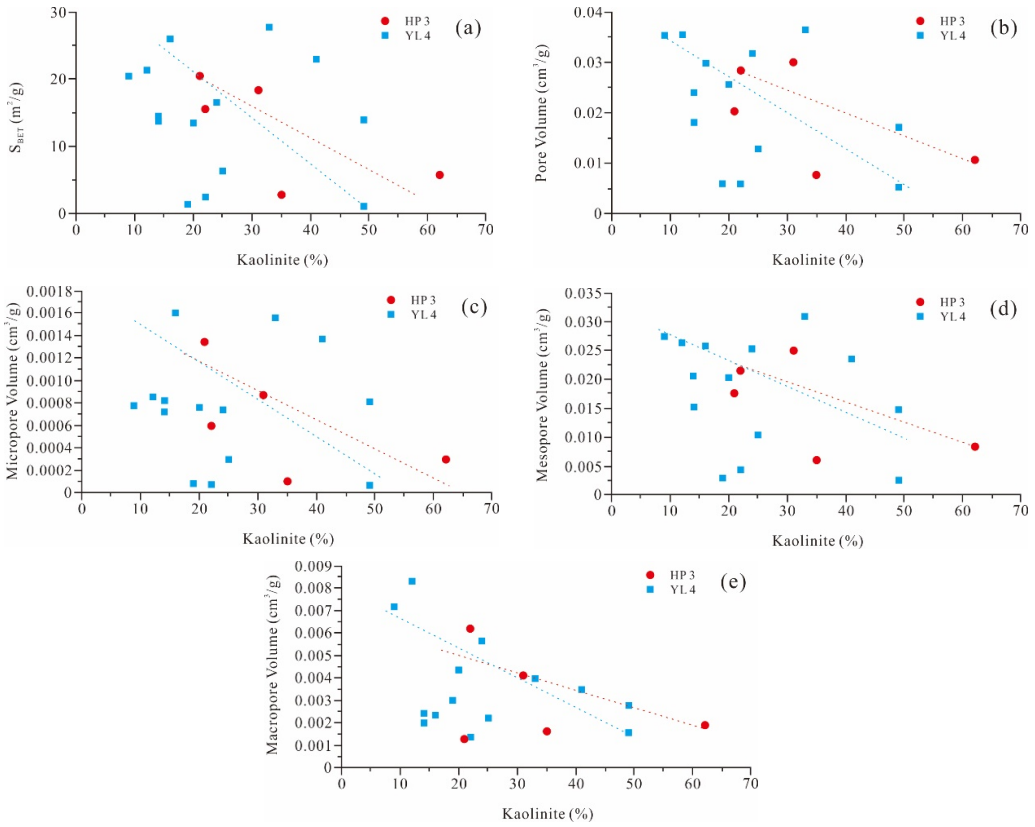

Figure 16. Relationship between pore structure characteristics and kaolinite.

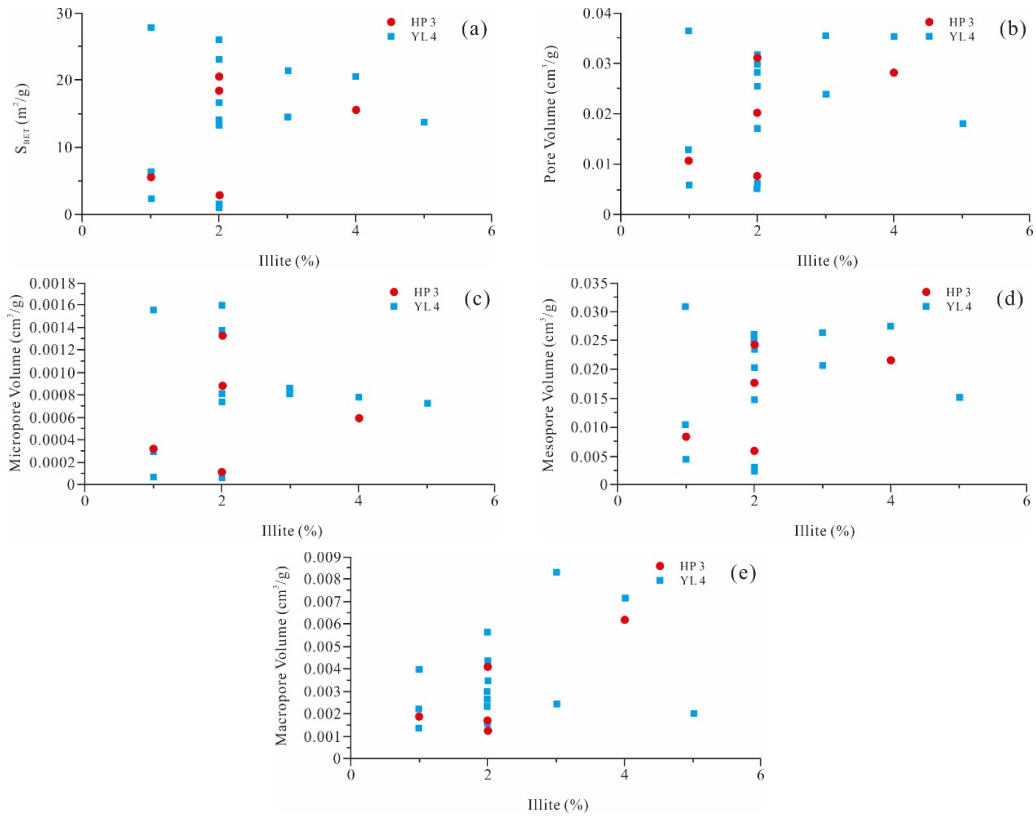

Figure 17. Relationship between pore structure characteristics and illite.

5.2. The Influence of Organic Matter on Pore Development

5.2.1. Relationship between Pore Structure Characteristics and TOC Content

During the process of hydrocarbon generation and expulsion, organic matter can produce large amounts of micro–nanopores, which has important implications for increasing reservoir adsorption and storage space and improving the permeability [38]. The Longtan Shale organic matter content is relatively high in western Guizhou. The organic matter content varies between 1.10% and 16.70% and averages at 5.43%. Unlike marine shale, where the kerogen types are type I and type II_1, and the macerals are mostly sapropelinite. The organic matter of marine and continental transitional shale in western Guizhou mainly originates from higher plant detritus, including type III and type II_2 kerogen; moreover, the maceral components are mainly vitrinite. Ungerer et al. found that the chemical structure of vitrinite has more aromatic and benzene rings, and its molecular structure is stable [39]. It is not easy to phase change and form thermogenic pores; thus, the organic pores are undeveloped. The SSA, micropore volume, mesopore volume, and total pore volume all decrease with the increasing TOC content of the Longtan Shale (Figure 18a–d). There was no correlation found between the macropore volume and TOC content (Figure 18e). This indicates that the contribution of TOC content to the SSA and pore volume is poor. In the Longtan Shale, the organic pores are relatively small in number and size, and the intergranular and intergranular pores are relatively developed (Figure 3f). This may be an important reason as to why no obvious negative correlation was found between the total pore volume and the TOC content [40]. Moreover, the shale plasticity will be strengthened due to the higher organic matter content, and it is more prone to mechanical compaction, which is adverse to pore preservation. In addition, excessive organic matter content will fill some inorganic mineral intergranular pores, thus further reducing the pore volume of the shale.

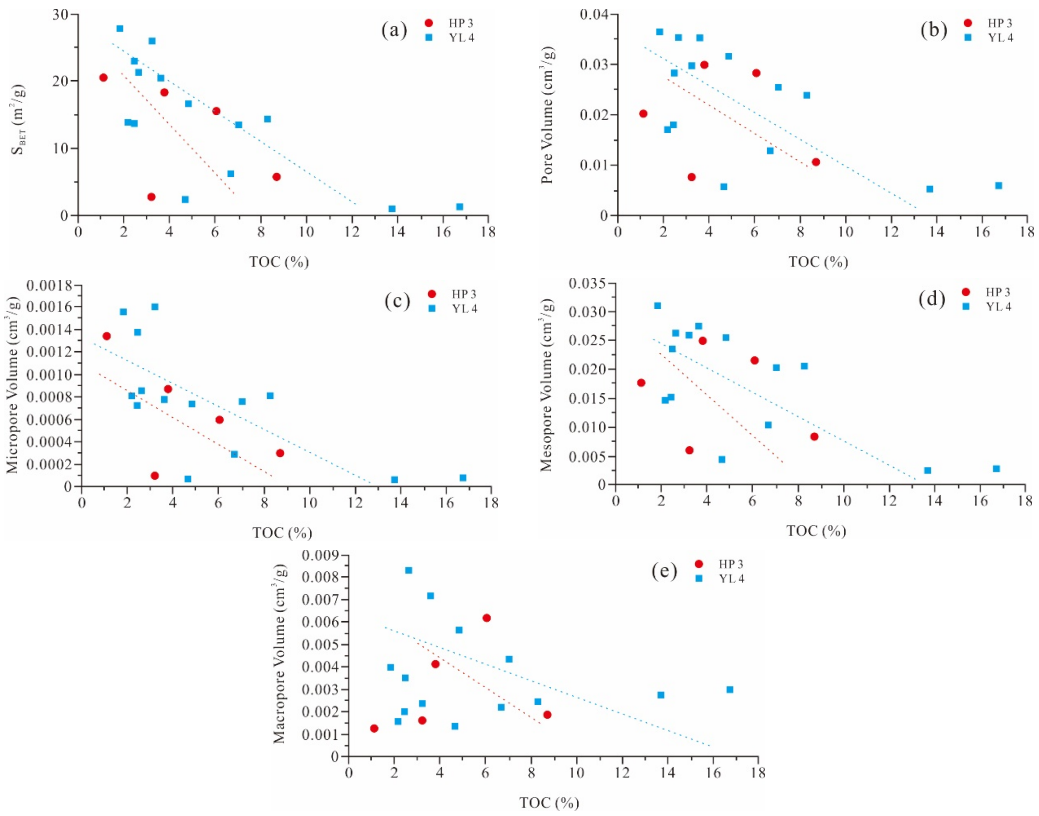

Figure 18. Relationship between the pore structure characteristics and TOC content.

5.2.2. Relationship between Pore Structure Characteristics and the Thermal-Evolution Degree

In shale, organic pore morphology and the degree of development are directly correlated with the hydrocarbon-generation evolution stage [40]. Curtis et al. (2012) believed that kerogen can only develop a great many nanoscale pores when it reaches a certain maturity, and immature-to-low-mature kerogen (R_o < 1.0%) has not undergone the pyrolysis and hydrocarbon expulsion process needed to remain in the original state of no pores or only a few pores [41,42]. Loucks et al. [25] and Curtis et al. [41] also found that when the thermal-evolution degree was less than 0.9%, no organic pores, or particularly few organic pores, were found in the shale SEM images. In accordance with this, undeveloped organic pores were also observed under the microscope in the Longtan Shale (Figure 3e,f).

The Longtan Shale vitrinite reflectance varies from 0.736% to 1.06% and averages at 0.92%. This is a mature evolution and occurs during the middle diagenetic stage; furthermore, this process mainly develops non-organic pores. As shown in Figure 19, the pore structure parameters of the Longtan Shale are irrelevant to thermal maturity (R_o), indicating that thermal maturity has no significant control over the non-organic SSA and pore volume. Loucks et al. and Zhang Y.F. et al. believed that the non-organic pores were mainly formed under the control of diagenesis [10,43], and the gradual increase in burial depth and paleogeotemperature, while the compaction was also more intense, led to the increase in thermal maturity. The strong compaction resulted in the deformation of the plastic minerals and the reduction in mineral pores. However, rigid particles can protect mineral pores from compaction, and mineral composition also has important effects on the non-organic pore evolution [44]. Moreover, cementation and clay mineral transformation also have destructive effects on mineral pores, while dissolution increases the number of mineral pores [43]. In conclusion, thermal maturity has little influence on the non-organic pore-evolution process of the Longtan Shale.

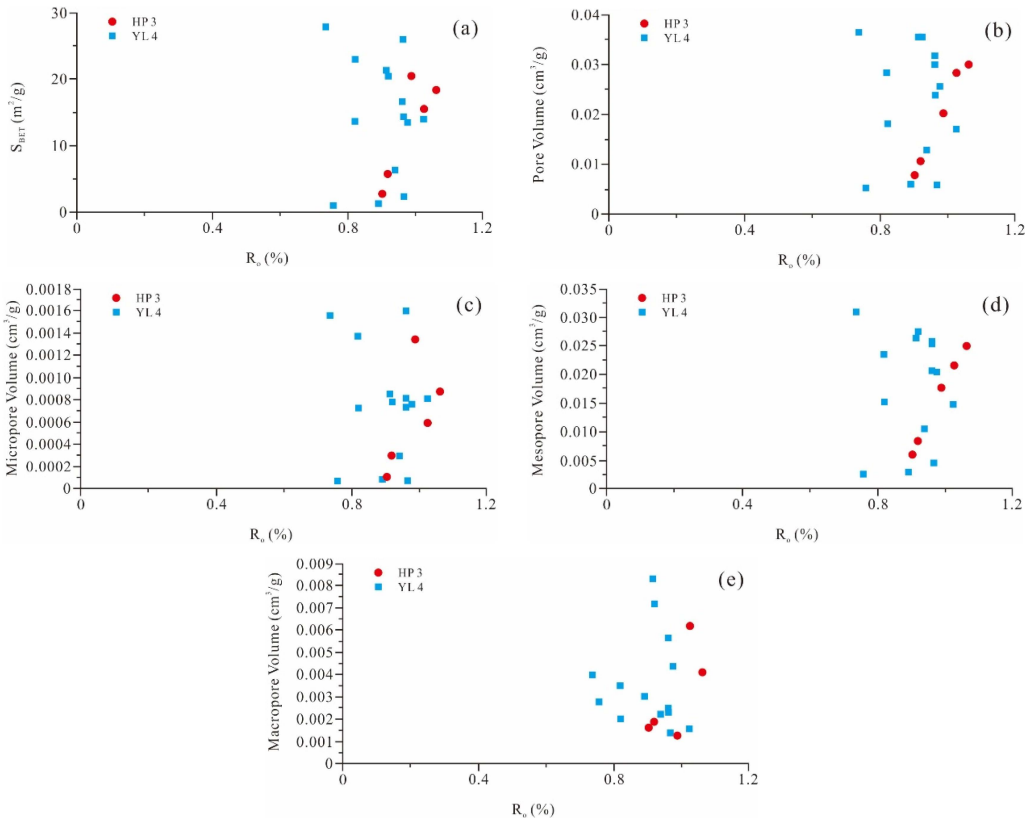

Figure 19. Relationship between the pore structure characteristics and vitrinite reflectance.

6. Conclusions

The physical properties and characteristics of the Upper Permian Longtan Shale pores in western Guizhou were studied, and the relationship between shale pore structure and physical properties was discussed. The following conclusions were made:

(1) The Longtan Shale mineral composition mainly consists of clay minerals and brittle minerals. In addition, the TOC content is rich, and the thermal maturity is low, which is the case due to the processes the shale underwent during its mature evolution stage and the peak of its gas generation period. The shale pore type includes intergranular pores, intragranular pores, organic pores, and microfractures. The intergranular pore structures are of the slit, layered, irregular, and ink-bottle varieties. The intragranular pores range from elliptical, nearly circular, ink-bottle, to irregular types. The organic pores are of the elliptical, bubble-like, and irregular polygonal variants. The microfractures are the elongated type. The clay-mineral-related intergranular pore is the predominant pore type, and it is mainly of the ink-bottle, slit, and layered varieties. The organic pores were found to be poorly developed.

(2) The Longtan Shale pores are mainly mesopores, followed by macropores. The development scale range of the pore diameter is large, ranging from 1 nm to 100 nm, with multiple peak characteristics. The nanopores mainly contributed to the SSA, which varied between 5 nm and 10 nm. The smaller pores provided a greater contribution to the SSA, which is more conducive to shale gas adsorption and accumulation.

(3) Clay mineral content is the dominant internal factor controlling pore development and the SSA, with the most obvious control being due to the illite–smectite mixed layer. However, too low or too high clay mineral content is adverse to macropore development. The macropore volume shows a tendency to first increase and then decrease with increasing clay mineral content. Brittle mineral content, carbonate mineral content, and TOC content are adverse to pore development and the SSA. Thermal maturity has no remarkable control effect on pore volume and the SSA of non-organic pores.

Author Contributions: Writing-original draft, investigation, M.Z.; supervision, M.H.; writing-review & editing, Funding acquisition, S.W.; investigation, Funding acquisition, Q.C.; Data curation, W.F. and F.S.; Visualization, L.Z.; Software, H.D. All authors have read and agreed to the published version of the manuscript.

Funding: This research was funded by Natural Science Foundation of Hubei Province: 2022CFB652 and China National Petroleum Corporation Innovation Found: 2021DQ02-0101.

Data Availability Statement: The data that support the findings of this study are available from the corresponding author upon reasonable request.

Conflicts of Interest: The authors declare no conflict of interest.

References

1. Li, J.; Li, H.; Yang, C.; Wu, Y.; Gao, Z.; Jiang, S. Geological Characteristics and Controlling Factors of Deep Shale Gas Enrichment of the Wufeng-Longmaxi Formation in the Southern Sichuan Basin, China. *Lithosphere* **2022**, *2022*, 4737801. [CrossRef]
2. Xi, Y.; Li, J.; Liu, G.; Cha, C.; Fu, Y. Numerical Investigation for Different Casing Deformation Reasons in Weiyuan-Changning Shale Gas Field during Multistage Hydraulic Fracturing. *J. Pet. Sci. Eng.* **2018**, *163*, 691–702. [CrossRef]
3. Gou, Q.; Xu, S.; Hao, F.; Zhang, B.; Shu, Z.; Yang, F.; Wang, Y.; Li, Q. Quantitative Calculated Shale Gas Contents with Different Lithofacies: A Case Study of Fuling Gas Shale, Sichuan Basin, China. *J. Nat. Gas Sci. Eng.* **2020**, *76*, 103222. [CrossRef]
4. Fu, W.; Hu, W.; Yi, T.; Kane, O.I.; Zhang, M.; Huang, X. Fractal Dimension Analysis of Pores in Coal Reservoir and Their Impact on Petrophysical Properties: A Case Study in the Province of Guizhou, SW China. *Minerals* **2022**, *12*, 1425. [CrossRef]
5. Fan, C.; Li, H.; Qin, Q.; He, S.; Zhong, C. Geological Conditions and Exploration Potential of Shale Gas Reservoir in Wufeng and Longmaxi Formation of Southeastern Sichuan Basin, China. *J. Pet. Sci. Eng.* **2020**, *191*, 107138. [CrossRef]
6. Wu, J.; Yuan, Y.; Niu, S.; Wei, X.; Yang, J. Multiscale Characterization of Pore Structure and Connectivity of Wufeng-Longmaxi Shale in Sichuan Basin, China. *Mar. Pet. Geol.* **2020**, *120*, 104514. [CrossRef]

7. Li, X.; Wang, Y.; Lin, W.; Ma, L.; Liu, D.; Liu, J.; Zhang, Y. Micro-Pore Structure and Fractal Characteristics of Deep Shale from Wufeng Formation to Longmaxi Formation in Jingmen Exploration Area, Hubei Province, China. *J. Nat. Gas Geosci.* **2022**, *7*, 121–132. [CrossRef]
8. Yang, R.; He, S.; Yi, J.; Hu, Q. Nano-Scale Pore Structure and Fractal Dimension of Organic-Rich Wufeng-Longmaxi Shale from Jiaoshiba Area, Sichuan Basin: Investigations Using FE-SEM, Gas Adsorption and Helium Pycnometry. *Mar. Pet. Geol.* **2016**, *70*, 27–45. [CrossRef]
9. Wang, Y.; Cheng, H.; Hu, Q.; Liu, L.; Jia, L.; Gao, S.; Wang, Y. Pore Structure Heterogeneity of Wufeng-Longmaxi Shale, Sichuan Basin, China: Evidence from Gas Physisorption and Multifractal Geometries. *J. Pet. Sci. Eng.* **2022**, *208*, 109313. [CrossRef]
10. Loucks, R.G.; Reed, R.M.; Ruppel, S.C.; Hammes, U. Spectrum of Pore Types and Networks in Mudrocks and a Descriptive Classification for Matrix-Related Mudrock Pores. *AAPG Bull.* **2012**, *96*, 1071–1098. [CrossRef]
11. Bingsong, Y.U. Classification and Characterization of Gas Shale Pore System. *Earth Sci. Front.* **2013**, *20*, 211–220.
12. Rouquerol, J.; Avnir, D.; Fairbridge, C.W.; Everett, D.H.; Haynes, J.H.; Pernicone, N.; Ramsay, J.D.F.; Sing, K.S.W.; Unger, K.K. Recommendations for the Characterization of Porous Solids. *Int. Union Pure Appl. Chem.* **1994**, *66*, 1739–1758. [CrossRef]
13. Kotarba, M.J.; Curtis, J.B.; Lewan, M.D. Comparison of Natural Gases Accumulated in Oligocene Strata with Hydrous Pyrolysis Gases from Menilite Shales of the Polish Outer Carpathians. *Org. Geochem.* **2009**, *40*, 769–783. [CrossRef]
14. Jarvie, D. Evaluation of Hydrocarbon Generation and Storage in the Barnett Shale, Ft. Worth Basin, Texas©. In Proceedings of the Ellison Miles Memorial Symposium, Farmers Branch, TX, USA, 22–23 June 2004.
15. Cao, T.; Deng, M.; Song, Z.; Luo, H.; Hursthouse, A.S. Characteristics and Controlling Factors of Pore Structure of the Permian Shale in Southern Anhui Province, East China. *J. Nat. Gas Sci. Eng.* **2018**, *60*, 228–245. [CrossRef]
16. Sun, W.; Zuo, Y.; Wu, Z.; Liu, H.; Xi, S.; Shui, Y.; Wang, J.; Liu, R.; Lin, J. Fractal Analysis of Pores and the Pore Structure of the Lower Cambrian Niutitang Shale in Northern Guizhou Province: Investigations Using NMR, SEM and Image Analyses. *Mar. Pet. Geol.* **2019**, *99*, 416–428. [CrossRef]
17. Wang, T.; Tian, F.; Deng, Z.; Hu, H. Pore Structure and Fractal Characteristics of Wufeng–Longmaxi Formation Shale in Northern Yunnan–Guizhou, China. *Front. Earth Sci.* **2023**, *10*, 998958. [CrossRef]
18. Yuan, K.; Huang, W.; Chen, X.; Cao, Q.; Fang, X.; Lin, T.; Jin, C.; Li, S.; Wang, C.; Wang, T. The Whole-Aperture Pore Structure Characteristics and Their Controlling Factors of the Dawuba Formation Shale in Western Guizhou. *Processes* **2022**, *10*, 622. [CrossRef]
19. Luo, W.; Hou, M.; Liu, X.; Huang, S.; Chao, H.; Zhang, R.; Deng, X. Geological and Geochemical Characteristics of Marine-Continental Transitional Shale from the Upper Permian Longtan Formation, Northwestern Guizhou, China. *Mar. Pet. Geol.* **2018**, *89*, 58–67. [CrossRef]
20. Ma, X.; Guo, S. Study on Pore Evolution and Diagenesis Division of a Permian Longtan Transitional Shale in Southwest Guizhou, China. *Energy Sci. Eng.* **2021**, *9*, 58–79. [CrossRef]
21. Boyer, C.; Kieschnick, J.; Suarez-Rivera, R.; Lewis, R.E.; Waters, G. Producing Gas from Its Source. *Oilfield Rev.* **2006**, *18*, 36–49.
22. Lin, L.; Zhang, J.; Liu, J.; Long, P.; Tang, X. Favorable Depth Zone Selection for Shale Gas Prospecting. *Earth Sci. Front.* **2012**, *19*, 259–263.
23. Slatt, R.M.; O'Brien, N.R. Pore Types in the Barnett and Woodford Gas Shales: Contribution to Understanding Gas Storage and Migration Pathways in Fine-Grained Rocks. *AAPG Bull.* **2011**, *95*, 2017–2030. [CrossRef]
24. Sun, W.; Zuo, Y.; Wu, Z.; Liu, H.; Zheng, L.; Wang, H.; Shui, Y.; Lou, Y.; Xi, S.; Li, T.; et al. Pore Characteristics and Evolution Mechanism of Shale in a Complex Tectonic Area: Case Study of the Lower Cambrian Niutitang Formation in Northern Guizhou, Southwest China. *J. Pet. Sci. Eng.* **2020**, *193*, 107373. [CrossRef]
25. Loucks, R.G.; Reed, R.M.; Ruppel, S.C.; Jarvie, D.M. Morphology, Genesis, and Distribution of Nanometer-Scale Pores in Siliceous Mudstones of the Mississippian Barnett Shale. *J. Sediment. Res.* **2009**, *79*, 848–861. [CrossRef]
26. Ko, L.T.; Loucks, R.G.; Zhang, T.; Ruppel, S.C.; Shao, D. Pore and Pore Network Evolution of Upper Cretaceous Boquillas (Eagle Ford–Equivalent) Mudrocks: Results from Gold Tube Pyrolysis Experiments. *AAPG Bull.* **2016**, *100*, 1693–1722. [CrossRef]
27. Yang, C.; Xiong, Y.; Zhang, J.; Liu, Y.; Chen, C. Comprehensive Understanding of OM-Hosted Pores in Transitional Shale: A Case Study of Permian Longtan Shale in South China Based on Organic Petrographic Analysis, Gas Adsorption, and X-Ray Diffraction Measurements. *Energy Fuels* **2019**, *33*, 8055–8064. [CrossRef]
28. Liang, J.; Huang, W.; Wang, H.; Blum, M.J.; Chen, J.; Wei, X.; Yang, G. Organic Geochemical and Petrophysical Characteristics of Transitional Coal-Measure Shale Gas Reservoirs and Their Relationships with Sedimentary Environments: A Case Study from the Carboniferous-Permian Qinshui Basin, China. *J. Pet. Sci. Eng.* **2020**, *184*, 106510. [CrossRef]
29. Sing, K.S.W.; Everett, D.H.; Haul, R.A.W.; Moscou, L.; Pierotti, J.H.; Rouquerol, J.; Siemieniewska, T. Reporting Physisorption Data for Gas/Solid Systems with Special Reference to the Determination of Surface Area and Porosity. *Pure Appl. Chem.* **1985**, *57*, 603–619. [CrossRef]
30. Thommes, M.; Kaneko, K.; Neimark, A.V.; Olivier, J.P.; Rodriguez-Reinoso, F.; Rouquerol, J.; Sing, K.S.W. Physisorption of Gases, with Special Reference to the Evaluation of Surface Area and Pore Size Distribution (IUPAC Technical Report). *Pure Appl. Chem.* **2015**, *87*, 1051–1069. [CrossRef]
31. Chen, S.; Zhu, Y.; Wang, H.; Liu, H.; Wei, W.; Fang, J. Shale Gas Reservoir Characterisation: A Typical Case in the Southern Sichuan Basin of China. *Energy* **2011**, *36*, 6609–6616. [CrossRef]

32. Wang, J.; Guo, S. The Whole-Aperture Pore-Structure Characteristics of Marine-Continental Transitional Shale Facies of the Taiyuan and Shanxi Formations in the Qinshui Basin, North China. *Interpretation* **2019**, *7*, T547–T563. [CrossRef]
33. de Boer, J.H.; Everett, D.H.; Stone, F.S. *The Structure and Properties of Porous Materials*; Colston Papers; Academic Press: Cambridge, MA, USA, 1958; Volume 90.
34. Chen, Y.; Qin, Y.; Wei, C.; Huang, L.; Shi, Q.; Wu, C.; Zhang, X. Porosity Changes in Progressively Pulverized Anthracite Subsamples: Implications for the Study of Closed Pore Distribution in Coals. *Fuel* **2018**, *225*, 612–622. [CrossRef]
35. Li, A.; Ding, W.; Jiu, K.; Wang, Z.; Wang, R.; He, J. Investigation of the Pore Structures and Fractal Characteristics of Marine Shale Reservoirs Using NMR Experiments and Image Analyses: A Case Study of the Lower Cambrian Niutitang Formation in Northern Guizhou Province, South China. *Mar. Pet. Geol.* **2018**, *89*, 530–540. [CrossRef]
36. Vishal, V.; Chandra, D.; Bahadur, J.; Sen, D.; Hazra, B.; Mahanta, B.; Mani, D. Interpreting Pore Dimensions in Gas Shales Using a Combination of SEM Imaging, Small-Angle Neutron Scattering, and Low-Pressure Gas Adsorption. *Energy Fuels* **2019**, *33*, 4835–4848. [CrossRef]
37. Hazra, B.; Wood, D.A.; Vishal, V.; Varma, A.K.; Sakha, D.; Singh, A.K. Porosity Controls and Fractal Disposition of Organic-Rich Permian Shales Using Low-Pressure Adsorption Techniques. *Fuel* **2018**, *220*, 837–848. [CrossRef]
38. Xi, Z.; Tang, S.; Li, J.; Zhang, Z.; Xiao, H. Pore Characterization and the Controls of Organic Matter and Quartz on Pore Structure: Case Study of the Niutitang Formation of Northern Guizhou Province, South China. *J. Nat. Gas Sci. Eng.* **2019**, *61*, 18–31. [CrossRef]
39. Ungerer, P.; Collell, J.; Yiannourakou, M. Molecular Modeling of the Volumetric and Thermodynamic Properties of Kerogen: Influence of Organic Type and Maturity. *Energy Fuels* **2015**, *29*, 91–105. [CrossRef]
40. Mastalerz, M.; Schimmelmann, A.; Drobniak, A.; Chen, Y. Porosity of Devonian and Mississippian New Albany Shale across a Maturation Gradient: Insights from Organic Petrology, Gas Adsorption, and Mercury Intrusion. *AAPG Bull.* **2013**, *97*, 1621–1643. [CrossRef]
41. Curtis, M.E.; Cardott, B.J.; Sondergeld, C.H.; Rai, C.S. Development of Organic Porosity in the Woodford Shale with Increasing Thermal Maturity. *Int. J. Coal Geol.* **2012**, *103*, 26–31. [CrossRef]
42. Chandra, D.; Vishal, V.; Bahadur, J.; Agrawal, A.K.; Das, A.; Hazra, B.; Sen, D. Nano-Scale Physicochemical Attributes and Their Impact on Pore Heterogeneity in Shale. *Fuel* **2022**, *314*, 123070. [CrossRef]
43. Zhang, Y.; Yu, B.; Pan, Z.; Hou, C.; Zuo, Q.; Sun, M. Effect of Thermal Maturity on Shale Pore Structure: A Combined Study Using Extracted Organic Matter and Bulk Shale from Sichuan Basin, China. *J. Nat. Gas Sci. Eng.* **2020**, *74*, 103089. [CrossRef]
44. Ross, D.J.K.; Marc Bustin, R. The Importance of Shale Composition and Pore Structure upon Gas Storage Potential of Shale Gas Reservoirs. *Mar. Pet. Geol.* **2009**, *26*, 916–927. [CrossRef]

Disclaimer/Publisher's Note: The statements, opinions and data contained in all publications are solely those of the individual author(s) and contributor(s) and not of MDPI and/or the editor(s). MDPI and/or the editor(s) disclaim responsibility for any injury to people or property resulting from any ideas, methods, instructions or products referred to in the content.